Article

SOURCE DATA | TRANSPARENT PROCESS

EMBO reports

Enhancing Spns2/S1P in macrophages alleviates hyperinflammation and prevents immunosuppression in sepsis

Chao Fang[1,†], Pan Ren[2,†], Ganlan Bian[3,†], Jian Wang[4], Jiaxin Bai[1], Jiaxing Huang[1], Yixiao Ding[1], Xueyong Li[2,*], Mingkai Li[1,**] & Zheng Hou[1,***]

Abstract

Sepsis is a leading cause of in-hospital mortality resulting from a dysregulated response to infection. Novel immunomodulatory therapies targeting macrophage metabolism have emerged as an important focus for current sepsis research. However, understanding the mechanisms underlying macrophage metabolic reprogramming and how they impact immune response requires further investigation. Here, we identify macrophage-expressed Spinster homolog 2 (Spns2), a major transporter of sphingosine-1-phosphate (S1P), as a crucial metabolic mediator that regulates inflammation through the lactate-reactive oxygen species (ROS) axis. Spns2 deficiency in macrophages significantly enhances glycolysis, thereby increasing intracellular lactate production. As a key effector, intracellular lactate promotes pro-inflammatory response by increasing ROS generation. The overactivity of the lactate-ROS axis drives lethal hyperinflammation during the early phase of sepsis. Furthermore, diminished Spns2/S1P signaling impairs the ability of macrophages to sustain an antibacterial response, leading to significant innate immunosuppression in the late stage of infection. Notably, reinforcing Spns2/S1P signaling contributes to balancing the immune response during sepsis, preventing both early hyperinflammation and later immunosuppression, making it a promising therapeutic target for sepsis.

Keywords immunomodulation; macrophages; sepsis; sphingosine-1-phosphate; Spinster homolog 2

Subject Categories Immunology; Metabolism; Signal Transduction

DOI 10.15252/embr.202256635 | Received 9 December 2022 | Revised 29 May 2023 | Accepted 13 June 2023 | Published online 26 June 2023

EMBO Reports (2023) 24: e56635

See also: **T Vanderhaeghen *et al*** (August 2023)

Introduction

Sepsis is a severe syndrome characterized by multiorgan dysfunction resulting from the host's dysregulated response to infection, making it a leading cause of in-hospital mortality (Singer *et al*, 2016; Rudd *et al*, 2020). Typically, the immune response in sepsis comprises two phases: an initial pro-inflammatory phase followed by a compensatory anti-inflammatory phase that can progress to immunosuppression (van der Poll *et al*, 2017). Immunosuppression can occur concurrently with the initial inflammation or develop later and increases morbidity and mortality due to unresolved septic foci and susceptibility to secondary infections (Torgersen *et al*, 2009; Otto *et al*, 2011; Hotchkiss *et al*, 2013; Venet & Monneret, 2018). Macrophages, as the first line of defense against infection, play a critical role in regulating the intensity of the immune response. While macrophage-mediated hyperinflammation can lead to early death through cardiovascular collapse, metabolic derangements, and multiple organ dysfunction during sepsis, premature reprogramming of macrophages from a pro-inflammatory to an anti-inflammatory phenotype contributes to the pathogenesis of immunosuppression (Hotchkiss *et al*, 2016; Venet *et al*, 2021). Currently, novel immunotherapy approaches have become a focus of sepsis research, with the aim of restoring or enhancing the immune system's normal function to improve septic patients' outcomes (Steinhagen *et al*, 2020).

Recent studies have shed light on the crucial role of cellular metabolism in macrophage reprogramming during sepsis (Shalova *et al*, 2015; Cheng *et al*, 2016; Bailey *et al*, 2019; Xu *et al*, 2022). Upon activation, macrophages undergo a significant metabolic switch from oxidative phosphorylation (OXPHOS) to aerobic glycolysis to support rapid energy production for an adequate inflammatory response (Rosenberg *et al*, 2022). One of the major metabolic

1 Department of Pharmacology, School of Pharmacy, Fourth Military Medical University, Xi'an, China
2 Department of Burns and Plastic Surgery, Tangdu Hospital, Fourth Military Medical University, Xi'an, China
3 Institute of Medical Research, Northwestern Polytechnical University, Xi'an, China
4 Department of Neurobiology, School of Basic Medicine, Fourth Military Medical University, Xi'an, China
*Corresponding author. Tel: +86 29 84777738; E-mail: yuyong@fmmu.edu.cn
**Corresponding author. Tel: +86 29 84774555; E-mail: mingkai@fmmu.edu.cn
***Corresponding author. Tel: +86 29 84774555; E-mail: houzheng@fmmu.edu.cn
†These authors contributed equally to this work

byproducts of glycolysis is lactate, and recent research has unveiled its immunomodulatory effects on macrophages (Nolt *et al*, 2018; Murray, 2020; Caslin *et al*, 2021). Most studies to date have focused on the inhibitory roles of extracellular lactate on macrophage-mediated inflammation, as elevated lactate levels in sepsis are associated with impaired immune response (Dietl *et al*, 2010; Hoque *et al*, 2014; Peter *et al*, 2015; Errea *et al*, 2016; Yang *et al*, 2020). However, endogenous lactate production resulting from the metabolic switch in activated macrophages may have more direct effects. Intracellular lactate has been found to promote homeostasis in activated macrophages through histone lactylation, increasing the expression of anti-inflammatory genes during late polarization (Zhang *et al*, 2019). In addition to its inhibitory effects, recent research suggests that endogenous lactate is required for NLRP3 inflammasome activation, pointing to a positive role for lactate in inflammation (Lin *et al*, 2021). Further research is necessary to fully comprehend how intracellular lactate affects macrophage function, particularly in the early stages of the inflammatory response.

Sphingosine-1-phosphate (S1P) is a crucial bioactive sphingolipid synthesized from sphingosine via sphingosine kinases (SphK1 and SphK2) and is primarily produced by endothelial cells, red blood cells (RBCs), and platelets. S1P functions as an essential ligand activating five isoforms of S1P receptors (S1PR1–5), which modulate various biological processes such as immune response, angiogenesis, cancer, and neurodegeneration (Cartier & Hla, 2019). The roles of S1P depend heavily on the presence of S1P transporters Spinster homolog 2 (Spns2), highly expressed by endothelial cells, and major facilitator superfamily domain-containing protein 2B (Mfsd2b), predominantly expressed by RBCs and platelets (Fukuhara *et al*, 2012; Vu *et al*, 2017). These transporters establish micromolar S1P concentration in circulatory fluids like plasma and lymph while maintaining low tissue levels, creating a gradient that facilitates lymphocyte egress from lymphoid organs into vasculature. This mechanism presents a potential therapeutic target for autoimmune diseases such as multiple sclerosis, psoriasis, asthma, rheumatoid arthritis, and transplantation (Fukuhara *et al*, 2012; Simmons & Ishii, 2014).

There is still much to uncover about how S1P signaling affects macrophage function, particularly in the context of bacterial infection. Studies have indicated that S1PR2 activation can promote macrophage pyroptosis while simultaneously suppressing macrophage phagocytosis and impairing the host's defense against sepsis (Hou *et al*, 2015; Song *et al*, 2018). Inhibiting the S1PR2 pathway, however, can be effective in reducing inflammation damage and increasing bacterial clearance, ultimately improving survival in sepsis models. Conversely, activating S1PR3 fosters phagosome maturation and enhances cellular bactericidal activity by mediating macrophage ROS generation (Hou *et al*, 2017). Although S1P signaling appears promising as a therapeutic target for sepsis (Winkler *et al*, 2017), many specifics regarding how it contributes to the development and progression of sepsis remain unknown. For instance, the upstream source of S1P and the downstream targets of S1P signaling that modulate macrophage functions during sepsis require further elucidation.

In this study, we have identified Spns2 expressed by macrophages as an essential immunomodulator that affects macrophage function during bacterial infection. We propose that the activation of S1P signaling by macrophage-expressed Spns2 through S1P autocrine/paracrine plays a crucial role in regulating the metabolic switch. The deficiency of Spns2 leads to a significant enhancement of glycolysis in macrophages, even under basal conditions. This occurs due to the malfunctioning of the malate–aspartate shuttle (MAS), which is responsible for transporting NADH generated in the cytosol to the mitochondria (Sanin *et al*, 2018). This disturbance in MAS caused by Spns2 deficiency further leads to mitochondrial reorganization and enhanced glycolysis (Willems *et al*, 2015; Wang *et al*, 2022). Notably, these changes in resting macrophages with Spns2 deficiency resemble those in activated macrophages, indicating that Spns2 may potentially participate in the metabolic switch after infection. The increased glycolysis leads to higher production of intracellular lactate, which positively promotes macrophage-mediated inflammation during bacterial infection. We found that the pro-inflammatory effects of intracellular lactate are closely linked to the production of oxidants that further promote the expression of inflammatory cytokines in the early phase of bacterial infection. In *Spns2*$^{-/-}$ sepsis models, lethal hyperinflammation can be observed, which can be attributed to the increased production of intracellular lactate in macrophages. However, in later stages of infection, severe innate immunosuppression occurs in sepsis models with Spns2 deficiency, which can be effectively rescued by strengthening S1P signaling. Therefore, Spns2/S1P signaling deficiency is probably a vital mechanism of both sepsis-induced hyperinflammation and immunosuppression, providing a potential therapeutic target to improve outcomes in septic patients.

Results

Spns2 deficiency results in an intense but quickly suppressed innate immune response during sepsis

Initially, we assessed the impact of Spns2 on sepsis model outcomes using transgenic rats with a global deletion of *Spns2*. Sepsis was induced through cecal ligation and puncture (CLP), resulting in rapid and high mortality among *Spns2*$^{-/-}$ rats. Within 12 h, the survival rate had dropped below 50%, and none survived after 24 h. In contrast, about one-third of wild-type (WT) rats survived after 72 h (Fig 1A). We evaluated bacterial loads in livers and spleens and found that the number of colony-forming units (CFUs) was lower in septic *Spns2*$^{-/-}$ rats than in WT rats at 4-h post-CLP but significantly increased at 8 and 12 h (Fig 1B). These findings were consistent with serum cytokine concentrations, indicating that levels of tumor necrosis factor α (TNFα), interleukin-1β (IL-1β), and IL-6 in *Spns2*$^{-/-}$ rats were higher or comparable to those of WT rats in the initial stage of sepsis (within 4-h post-CLP) but decreased dramatically later (Fig 1C). The premature reduction of pro-inflammatory cytokines indicated early innate immunosuppression in the absence of Spns2, despite the initial intensive response during sepsis. Meanwhile, septic *Spns2*$^{-/-}$ rats exhibited worse pathological lung changes at 12 h compared with WT rats (Fig 1D), suggesting an overwhelmed systemic infection in *Spns2*$^{-/-}$ rats likely accounted for their rapid deaths.

However, the lack of supportive therapeutic interventions poses a major challenge in bridging the gap between experimental sepsis models and clinical sepsis. Therefore, it is essential to use supportive treatments like fluid resuscitation and antibiotic treatment to

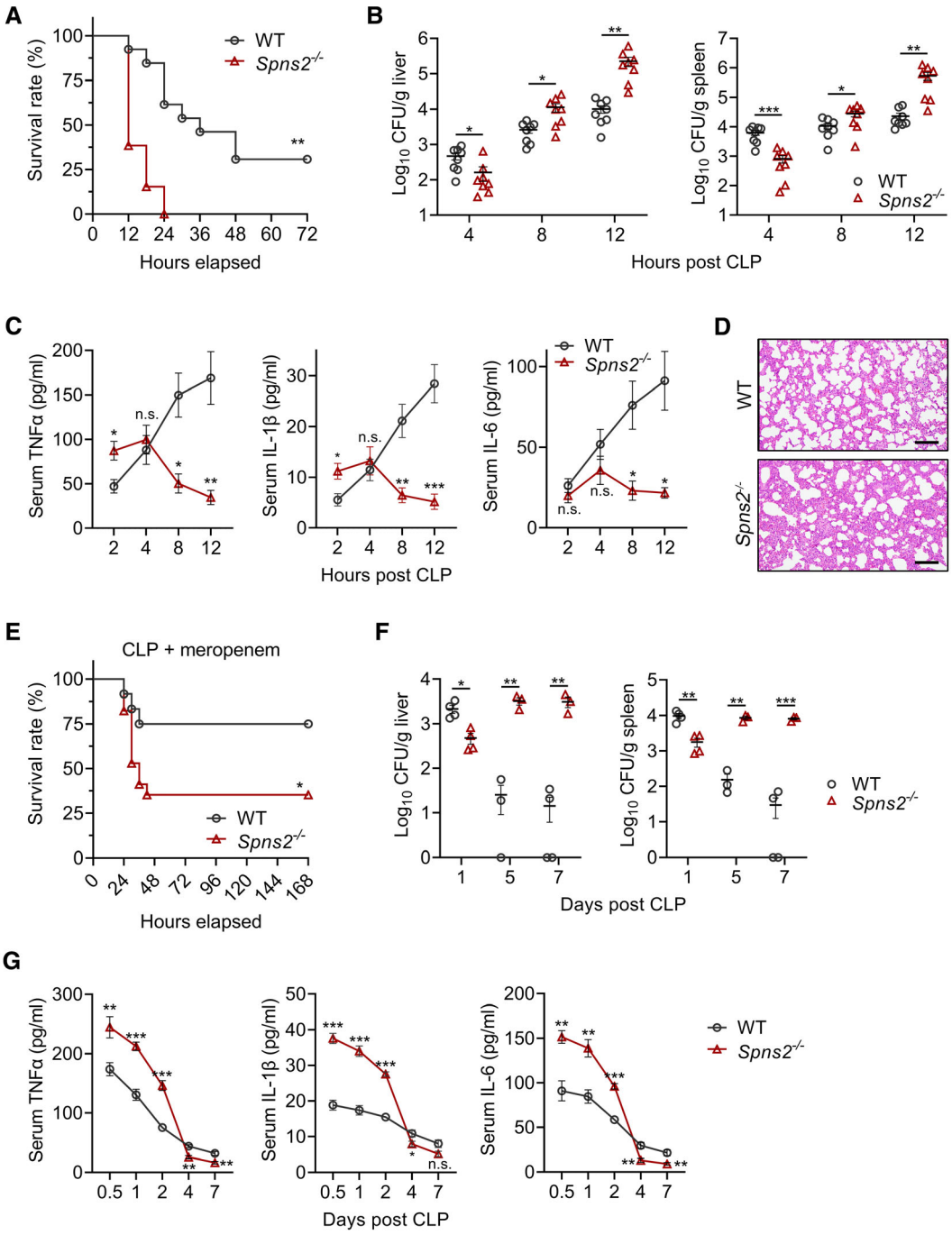

Figure 1. Spns2 deficiency results in early hyperinflammation and subsequent immunosuppression during sepsis.

A Survival curves for WT and *Spns2*$^{-/-}$ CLP models without antibiotic therapy within 72 h (n = 13 for each group).
B CFU counting in livers and spleens of CLP models without antibiotic therapy (n = 8 per time point for each group).
C Concentrations of serum cytokines in CLP models without antibiotic therapy (n = 6 per time point for each group).
D H&E staining of lungs from sepsis models without antibiotic therapy at 12-h post-CLP. Scale bars: 100 μm.
E Survival curves for WT (n = 12) and *Spns2*$^{-/-}$ (n = 17) CLP models receiving meropenem treatment within 7 days.
F CFU counting in livers and spleens of meropenem-treated CLP models (n = 3 to 4 per time point for each group).
G Concentrations of serum cytokines in meropenem-treated CLP models (n = 6 per time point for each group).

Data information: Data are presented as percentage (A and E) and mean ± s.e.m. (B, C, F, and G). N represents biological replicates. P-values were determined by log-rank test (A and E) and unpaired t-test (B, C, F, and G). *P < 0.05; **P < 0.01; ***P < 0.001; n.s., not significant.
Source data are available online for this figure.

mimic human sepsis (Romero *et al*, 2010; Dejager *et al*, 2011). Here, we established the CLP models and administered fluid resuscitation and antibiotic treatment throughout the observation period. The antibiotic treatment significantly reduced the bacterial counts in the livers and spleens of both groups and improved their overall survival rates (Fig 1E and F). In the WT group, the survival rate was approximately 75% after 7-day post-CLP, and low infection levels were detected in their livers and spleens after 5 days. In the Spns2$^{-/-}$ models, the antibiotic treatment raised the survival rate to approximately 40% at 7-day post-CLP. Most *Spns2*$^{-/-}$ model deaths occurred within 48 h due to excessive inflammation. We observed significantly higher serum cytokine levels in the *Spns2*$^{-/-}$ models within 48 h, which dramatically decreased after 96 h (Fig 1G). It is worth noting that at the endpoint of observation (7 days), high levels of unresolved infection were still detected in the *Spns2*$^{-/-}$ models, indicating the occurrence of immunosuppression and likely resulting in late secondary infection and death after cessation of antibiotic treatment.

Cecal ligation and puncture is a classical model for polymicrobial sepsis, and the outcomes can be influenced by the composition of the microbiome in the cecum, which may vary between WT and *Spns2*$^{-/-}$ rats. Therefore, we established *Escherichia coli* (*E. coli*)-induced peritonitis models to investigate whether the phenotype could be attributed to antimicrobial effects or not. In the sepsis model triggered by a single high-dose *E. coli* infection, approximately 16% mortality rate was observed within 24 h in the WT group. In contrast, the *Spns2*$^{-/-}$ rats did not survive beyond 6 h (Fig EV1A), and the levels of serum TNFα, IL-1β, and IL-6 were considerably higher in *Spns2*$^{-/-}$ rats (Fig EV1B). These findings suggest that excessive inflammatory responses led to the fatal outcome. The injection of an equal amount of heat-killed *E. coli* further supported this observation, where all *Spns2*$^{-/-}$ rats died within 8–10 h while the WT rats survived (Fig EV1A and B). These observations were consistent with the hyperinflammation observed in CLP models with or without antibiotic therapy, indicating that Spns2 deficiency leads to an intense innate immune response during the early stages of sepsis, exacerbating inflammatory injury, and resulting in high mortality.

To replicate the gradual and continuous release of bacteria in CLP models, rats were repeatedly exposed to low-dose *E. coli* infection for 12 h. In this model, all *Spns2*$^{-/-}$ rats died within 36 h, while only approximately 10% of WT rats died within 48 h (Fig EV1C). The immune response pattern in this model resembled that of the CLP model without antibiotic therapy, with *Spns2*$^{-/-}$ rats experiencing immunosuppression after 8-h postinfection following the initial hyperinflammatory response (Fig EV1D). The compromised innate immune function in *Spns2*$^{-/-}$ rats was further assessed by a mild intraperitoneal challenge with *Salmonella typhimurium* (*S. typhimurium*), which causes intracellular infection and is primarily cleared by innate immune cells (West *et al*, 2011). The CFUs were not significantly different between both groups on the first and third day postinfection. However, *Spns2*$^{-/-}$ rats harbored approximately 5–10 times more bacteria on the fifth day than WT rats, reproducing the occurrence of immunosuppression in an *S. typhimurium*-infected model (Fig EV1E).

These findings reveal the dual roles of Spns2 in the innate immune response to bacterial challenges. On the one hand, Spns2 controls the intensity of the inflammatory response in the early phase of infection, and ablation of Spns2 enhances the production of pro-inflammatory cytokines and inhibitory efficacy on bacterial growth. On the other hand, Spns2 is crucial to sustaining inflammation in the later phase, and its dysfunction can potentially cause innate immunosuppression during sepsis.

Spns2 expression in macrophages plays a vital role in shaping the antibacterial response during sepsis

Spns2 is primarily expressed in endothelial cells, and its absence leads to a moderate reduction in blood-borne S1P (Mendoza *et al*, 2012; Nijnik *et al*, 2012; Obinata & Hla, 2019). We determined that the serum S1P concentration in *Spns2*$^{-/-}$ rats was approximately 75% of that in WT rats before infection and gradually decreased after 8-h post-CLP, following a comparable trend between both groups (Fig EV2A). However, it remained unclear whether the distinct features of sepsis-induced inflammation were attributable to differences in blood-borne S1P levels. We analyzed the correlations between serum S1P concentrations and pro-inflammatory cytokine levels during both the early (2–4 h, Fig EV2B) and later (4–12 h, Fig EV2C) phases of CLP models without antibiotic therapy. The results revealed very weak correlations, indicating that blood-borne S1P, mostly bound to high-density lipoprotein (HDL) and albumin (Obinata & Hla, 2019), was probably not a key mediator of sepsis-induced inflammation. Thus, we speculate that in this scenario, Spns2 expressed by innate immune cells but not by endothelial cells predominated.

We subsequently isolated peritoneal macrophages (PMs) and discovered that *Spns2* was expressed in WT PMs, with the gene expression level being approximately one-twentieth of that in endothelial cells (Fig EV2D). Notably, the transcriptional profiles of *Tnfα*, *Il1β*, and *Il6* in PMs stimulated with lipopolysaccharide (LPS) phenocopied the inflammatory response seen in sepsis models. LPS initially triggered higher levels of cytokine expression in *Spns2*$^{-/-}$ PMs but dramatically decreased thereafter (Figs 2A and EV2E). These results indicated the essential role of macrophage-expressed Spns2 in shaping the inflammatory response to bacterial infection. To eliminate the potential effects of Spns2 expressed by endothelial cells on the outcomes of sepsis models, we performed bone marrow transplantation between WT and *Spns2*$^{-/-}$ rats and evaluated the outcomes and inflammatory response in the septic transplanted models. The chimerism rates exceeded 95% in both groups (Appendix Fig S1). We established CLP models with or without antibiotic treatment, as well as live *E. coli*-induced sepsis models using the transplanted rats, and the outcomes of these models successfully reproduced the *in vivo* results obtained with both WT and *Spns2* global deletion rats. Regarding the CLP models without antibiotic therapy, all WT recipients died within 36 h, whereas the survival rate of *Spns2*$^{-/-}$ recipients was 30% within 72 h (Fig 2B). As we previously observed, at 2-h post-CLP, WT recipients exhibited a higher inflammatory response than *Spns2*$^{-/-}$ recipients, while concentrations of serum cytokines dropped to low levels at 12 h, indicating immunosuppression (Fig 2C). In CLP models with antibiotic therapy, the treatment significantly improved overall outcomes in both groups. The majority of deaths occurred within 48 h following the CLP procedure (Fig 2D). We found that serum inflammatory cytokine levels were higher in WT recipients than in *Spns2*$^{-/-}$ recipients at 24 h but significantly decreased on the seventh day

(Fig 2E). Consistently, we identified high levels of persistent infections in the livers and spleens of WT recipients but not in the organs of *Spns2*$^{-/-}$ recipients on the seventh day, further supporting our conclusion that Spns2 deficiency in macrophages affects bacterial clearance (Fig 2F). For live *E. coli*-induced sepsis models, all the WT recipients died within 6 h after bacterial infection, with significantly higher levels of serum inflammatory cytokines compared with the *Spns2*$^{-/-}$ recipients (Fig 2G and H). Furthermore, the co-cultures of PMs and endothelial cells using a transwell insert did not affect the inflammatory response of *Spns2*$^{-/-}$ PMs to LPS challenge (Fig EV2F). We hypothesize that S1P released by endothelial cells might have bound to chaperones in the culture medium, thus preventing efficient activation of S1P signaling in *Spns2*$^{-/-}$ macrophages. The results provide strong support for our suggestion that Spns2 expressed in macrophages, rather than endothelial cells, has a critical role in modulating the immune response during sepsis.

Spns2 deficiency impairs the malate–aspartate shuttle and causes a metabolic switch from OXPHOS to glycolysis in macrophages

We conducted RNA sequencing (RNA-seq) to investigate the impact of Spns2 on PMs under basal conditions. The RNA-seq analysis revealed 472 upregulated genes in *Spns2*$^{-/-}$ PMs (Fig EV3A, Dataset EV1), and Gene Ontology (GO) enrichment analysis indicated that the categories of response to hypoxia, glycolytic process, and response to oxidative stress were enhanced in the absence of Spns2 (Fig EV3B, Dataset EV2). Additionally, Kyoto Encyclopedia of Genes and Genomes (KEGG) enrichment analysis also demonstrated that glycolysis/gluconeogenesis was increased in *Spns2*$^{-/-}$ PMs under basal conditions (Fig EV3C, Dataset EV3). Hierarchical clustering highlighted a broad set of enzymes involved in glycolysis that were significantly increased in *Spns2*$^{-/-}$ PMs, indicating elevated aerobic glycolysis metabolism even before infection (Fig 3A). To confirm the shift from OXPHOS toward glycolysis in *Spns2*$^{-/-}$ PMs, we measured oxygen consumption rate (OCR), glucose consumption, the ratio of nicotinamide adenine dinucleotide (NAD^+) to the reduced form NADH, and lactate production in both genotypic PMs (Cheng *et al*, 2014). We found that *Spns2*$^{-/-}$ PMs had a marked reduction in basal, maximal, and ATP-coupled respiratory rates, whereas non-ATP-coupled oxygen consumption (proton leak) was slightly increased compared with WT PMs (Fig 3B). We also observed an increased glucose consumption, the ratio of NAD^+ to NADH, and intracellular lactate production, which further confirmed the metabolic switch in *Spns2*$^{-/-}$ PMs (Fig 3C). Importantly, supplementing 1 μM S1P effectively promoted the process of OXPHOS in *Spns2*$^{-/-}$ PMs (Fig 3B and C). This suggests that Spns2 plays an essential role in maintaining OXPHOS in PMs through the autocrine/paracrine mechanism of S1P, which likely influences the inflammatory response to bacterial infection.

The metabolic shift from OXPHOS to aerobic glycolysis is a characteristic feature of activated macrophages and is closely related to mitochondrial dynamics, which refers to the coordinated changes in mitochondrial morphology between fission and fusion (Xie *et al*, 2020; Schuster *et al*, 2021). We investigated whether the enhanced glycolysis in resting *Spns2*$^{-/-}$ PMs was due to the changes in mitochondrial dynamics. Transmission electron microscopy (TEM) revealed fragmented mitochondria in *Spns2*$^{-/-}$ PMs with shorter lengths and looser cristae (Fig 4A and B, Appendix Fig S2), significantly different from WT PMs. Using CytoFix™ MitoRed, a fluorescent probe independent of mitochondrial membrane potential ($\Delta\psi m$), we detected an increased mitochondrial mass in *Spns2*$^{-/-}$ PMs (Fig 4C). Meanwhile, MitoTracker™ Red staining, which is dependent on $\Delta\psi m$, also showed an increased intensity (Fig 4D). The ratio of MitoTracker™ Red to CytoFix™ MitoRed indicated the average $\Delta\psi m$, which was decreased in *Spns2*$^{-/-}$ PMs (Fig 4E), confirming compromised mitochondrial function in the absence of Spns2. Overall, *Spns2*$^{-/-}$ PMs exhibited fragmented mitochondrial morphology, loose cristae, increased mass, and reduced $\Delta\psi m$ under basal conditions, consistent with the mitochondrial remodeling seen during LPS challenge (Yu *et al*, 2020). We measured the expression of the main proteins involved in mitochondrial fusion and fission (Mishra & Chan, 2016; Wai & Langer, 2016) and found a significant increase in the levels of pro-fission molecules Drp1, p-Drp1^{S616}, and short-form Opa1 (S-Opa1) in *Spns2*$^{-/-}$ PMs, whereas the levels of pro-fusion molecules Mfn1 and long-form Opa1 (L-Opa1) were comparable (Fig 4F). Unexpectedly, the expression of Mfn2 increased in *Spns2*$^{-/-}$ PMs. A recent report showed that LPS stimulation induced Mfn2 expression in macrophages and highlighted its essential roles in metabolic adaptation and pro-inflammatory response (Tur *et al*, 2020). Thus, we considered the elevated Mfn2 expression consistent with our findings that resting *Spns2*$^{-/-}$ PMs undergo mitochondrial remodeling similar to the LPS-challenged state.

The observations in *Spns2*$^{-/-}$ macrophages suggest a possible link to impaired mitochondrial NADH shuttles, which transport NADH generated during glycolysis from the cytosol to the mitochondria to reduce molecular oxygen at complex IV of the electron transport chain (Wang *et al*, 2022). This process is essential for regenerating cytosolic NAD^+ and relies on the malate–aspartate shuttle (MAS) and glycerol 3-phosphate shuttle (G3PS; Sanin *et al*, 2018; Langston *et al*, 2019). If the amount of NADH shuttle is insufficient, it results in reduced $\Delta\psi m$ and mitochondrial fission, as well as an increase in lactate dehydrogenase (LDH) activity (Willems *et al*, 2015). The RNA-seq analysis showed a significant reduction in the gene expression of MAS components, but not G3PS in *Spns2*$^{-/-}$ PMs (Fig 4G). This finding was further confirmed by detecting the protein expression of Slc25a12 and Slc25a13 (Fig 4H). Importantly, supplementing with S1P reversed the reduced expression of Slc25a12 and Slc25a13 in *Spns2*$^{-/-}$ PMs (Fig 4H), suggesting that compromised MAS function may have caused the metabolic changes observed.

These findings demonstrate the crucial roles of Spns2/S1P signaling in mediating the metabolic switch of macrophages. Adequate activation of S1P signaling strengthened the function of MAS and promoted mitochondrial fusion to sustain the process of OXPHOS. Conversely, attenuated S1P signaling resulted in decreased MAS activity, facilitated mitochondrial fission, and enhanced aerobic glycolysis even under basal conditions.

Intracellular lactate drives augmented ROS generation in macrophages

It has been reported that mitochondrial remodeling in activated macrophages is responsible for the production of reactive oxygen species (ROS; Yu *et al*, 2020). GO enrichment analysis revealed an active gene expression in response to oxidative stress in *Spns2*$^{-/-}$

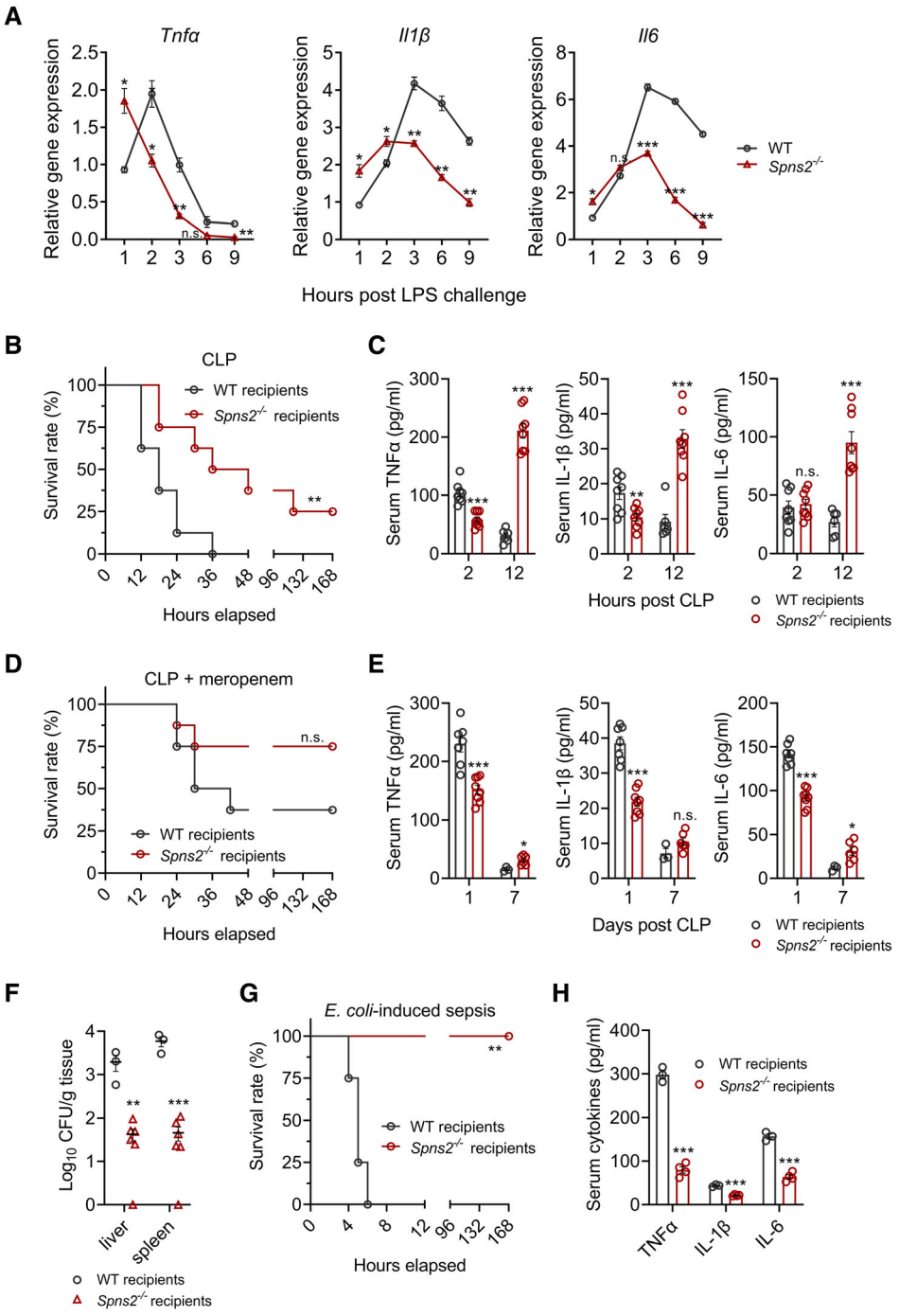

Figure 2.

Figure 2. Macrophage-expressed Spns2 is essential in shaping the inflammatory response during sepsis.

A Gene expression of inflammatory cytokines in isolated PMs challenged with 10 ng/ml LPS (n = 3 per time point for each group).
B Survival curves for bone marrow transplanted CLP models without antibiotic therapy within 7 days (n = 8 for each group).
C Concentrations of serum cytokines in bone marrow transplanted CLP models without antibiotic therapy (n = 6–8 per time point for each group).
D Survival curves for bone marrow transplanted CLP models receiving meropenem treatment within 7 days (n = 8 for each group).
E Concentrations of serum cytokines in meropenem-treated bone marrow transplanted CLP models (n = 3–8 per time point for each group).
F CFU counting in livers and spleens of meropenem-treated bone marrow transplanted CLP models on the seventh day (n = 3 for WT recipients; n = 6 for *Spns2*$^{-/-}$ recipients).
G Survival curves for bone marrow transplanted sepsis models induced by *E. coli* peritoneal infection within 7 days (n = 4 for each group).
H Concentrations of serum cytokines in bone marrow transplanted sepsis models at 5-h post-*E. coli* infection (n = 3 for WT recipients; n = 4 for *Spns2*$^{-/-}$ recipients).

Data information: Data are presented as percentage (B, D, and G) and mean ± s.e.m. (A, C, E, F, and H). N represents biological replicates. P-values were determined by log-rank test (B, D, and G) and unpaired t-test (A, C, E, F, and H). *P < 0.05; **P < 0.01; ***P < 0.001; n.s., not significant.
Source data are available online for this figure.

PMs, indicating that Spns2 plays a crucial role in regulating the redox state in PMs by affecting mitochondrial dynamics (Figs EV3B and 5A). We observed elevated levels of mitochondrial-derived ROS (mtROS) in *Spns2*$^{-/-}$ PMs (Fig 5B), while total intracellular ROS levels were similar between both groups (Fig 5C). This implied that the comparable total oxidant levels were likely due to the compensatory increase in antioxidative activity indicated by the RNA-seq results (Figs EV3B and 5A). We found that the total superoxide dismutase and catalase activities were enhanced in *Spns2*$^{-/-}$ PMs (Fig 5D). Furthermore, the protein levels of peroxiredoxin 1 (Prdx1) and Prdx6, known to play essential roles in protecting against oxidative stress (Espinosa-Diez *et al*, 2015; Ishii, 2015), were also upregulated in *Spns2*$^{-/-}$ PMs, suggesting cooperative antioxidant effects that maintain homeostasis in resting PMs (Fig 5E).

However, it is unclear how mitochondrial remodeling leads to an increase in ROS production. Under basal conditions, *Spns2*$^{-/-}$ PMs exhibited altered redox states, leading us to speculate that certain metabolic byproducts of glycolysis may play a fundamental role in this process. To investigate this further, we used rotenone, an inhibitor of the mitochondrial respiratory chain complex I, to shift WT PMs toward glycolysis (Kampjut & Sazanov, 2020). As the rotenone concentration increased, a corresponding rise in intracellular lactate level was observed (Fig 6A). In addition, the production of mtROS and the activities of superoxide dismutase and catalase increased in a concentration-dependent manner (Fig 6B and C). These results suggested that intracellular lactate may play an essential role in ROS generation. To confirm this hypothesis, we used oxamate, a lactate dehydrogenase inhibitor (Young *et al*, 2020), to reduce lactate production in *Spns2*$^{-/-}$ PMs (Fig 6D), which resulted in decreased production of mtROS (Fig 6E) as well as reduced activities of total superoxide dismutase and catalase (Fig 6F). Furthermore, we observed that supplementing with S1P effectively diminished oxidative stress in *Spns2*$^{-/-}$ PMs (Fig 6E and F). This effect can be attributed to the previously demonstrated decrease in intracellular lactate levels (Fig 3C). These findings suggest that mitochondrial remodeling induces ROS generation by increasing intracellular lactate levels and that Spns2/S1P signaling affects the redox state by regulating glycolysis-mediated lactate production.

The results of *in vivo* experiments demonstrate that CFUs in both liver and spleen were significantly lower in *Spns2*$^{-/-}$ CLP models during the early stages of sepsis, regardless of whether antibiotic therapy was administered (Fig 1B and F). This suggests a higher inhibitory efficacy on pathogens in the absence of Spns2 during the early phase of infection. We then investigated whether this phenomenon was associated with increased ROS production in activated *Spns2*$^{-/-}$ PMs. RNA-seq analysis showed significantly higher expression levels of *Nos2* and *Acod1* in activated *Spns2*$^{-/-}$ PMs at 3-h post-LPS challenge (Fig EV4A). These genes are known to induce the production of nitric oxide (NO) and mtROS, respectively (Wu *et al*, 2020). Furthermore, decreased gene expression of antioxidative molecules in both genotypic PMs indicated attenuated antioxidative activities after infection, which likely allowed for sufficient production of ROS and NO to exert bactericidal effects (Fig EV4B). Additionally, the observation that *Spns2*$^{-/-}$ PMs enhanced antioxidative activities to sustain homeostasis in the resting state reinforced our speculation that the attenuated antioxidative activities after activation led to more production of ROS and NO in activated *Spns2*$^{-/-}$ PMs. Indeed, the levels of total intracellular ROS, mtROS, and NO production were significantly higher in *Spns2*$^{-/-}$ PMs than WT PMs at 3-h postinfection (Fig 6G–I). The distinct antibacterial efficacy was further confirmed by challenging PMs with *S. typhimurium*, which revealed that intracellular replication of *S. typhimurium* was significantly lower in *Spns2*$^{-/-}$ PMs (Fig EV4C). These results highlight the pro-oxidative effects of intracellular lactate on PMs under both basal and activated conditions. Spns2 deficiency enhances glycolysis and causes the accumulation of intracellular lactate in resting PMs, which may promote ROS and NO production to exert higher efficacy against bacterial infection.

Spns2/S1P signaling alleviates hyperinflammation in sepsis by suppressing the lactate-ROS axis

We have discovered that the deficiency of Spns2 in macrophages results in an increase in intracellular lactate production, which further promotes the generation of ROS. It is worth noting that ROS generated by activated macrophages is crucial not only to eliminate bacteria but also to facilitate the production of pro-inflammatory cytokines (Weinberg *et al*, 2015; Tur *et al*, 2017, 2020). Therefore, we propose that the excessive and lethal inflammatory response observed in *Spns2*$^{-/-}$ rats during the early stages of sepsis may be attributed to the overactivity of the lactate-ROS axis. To test this hypothesis, we pretreated *Spns2*$^{-/-}$ PMs with either oxamate or mitoquinone to reduce intracellular lactate or mtROS levels, respectively. Our findings showed that both oxamate and mitoquinone effectively inhibited the gene expression of pro-inflammatory cytokines in a concentration-dependent manner (Fig 7A and B). These results confirm the crucial role of the lactate-ROS axis in mediating hyperinflammation in the context of bacterial infections.

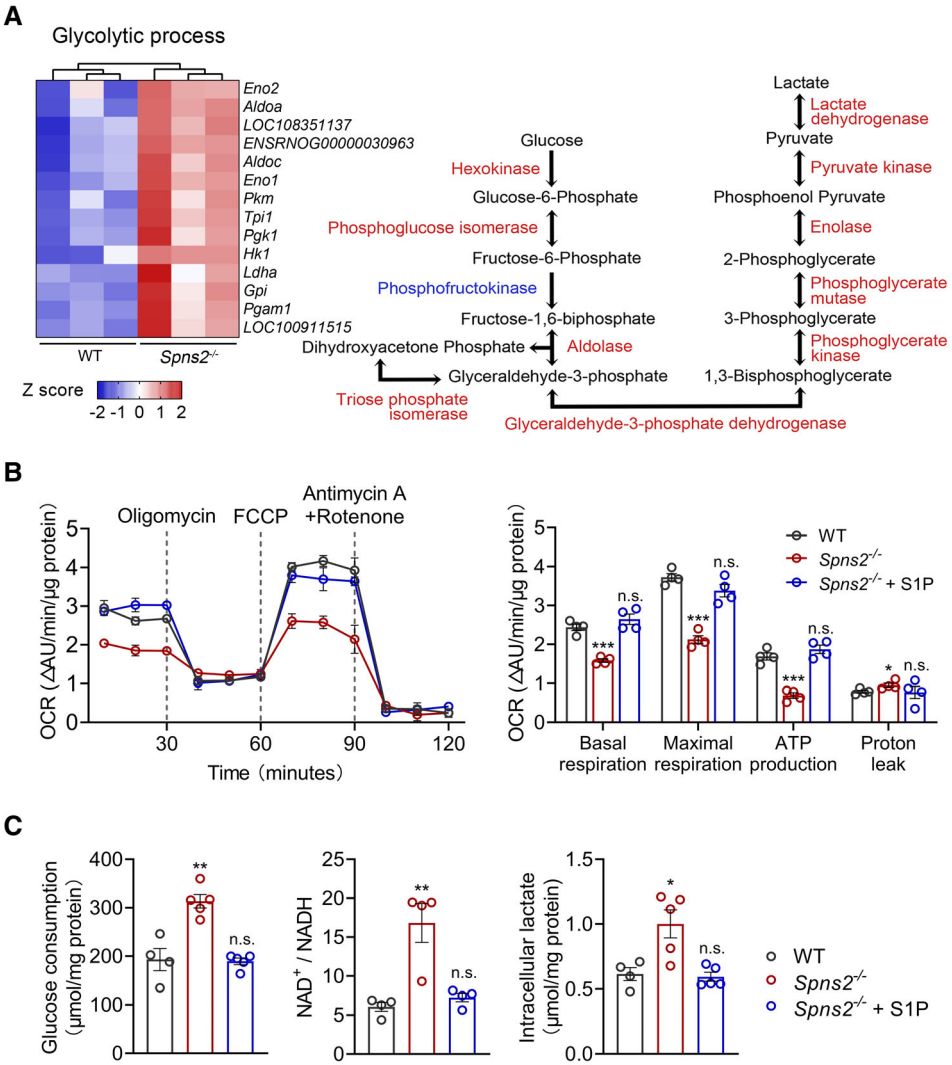

Figure 3. Peritoneal macrophages enhance glycolysis in the absence of Spns2.

A Heat map and schematic diagram highlighting the upregulated genes in *Spns2*$^{-/-}$ PMs associated with glycolysis. Red markings indicate upregulated enzymes, and blue markings indicate not significant (n = 3 for each group).

B Oxygen consumption rates (OCR) and quantifications of basal respiration, maximal respiration, ATP production, and proton leakage in resting WT, *Spns2*$^{-/-}$, and 1 μM S1P pretreated *Spns2*$^{-/-}$ PMs (n = 4 for each group).

C Total glucose consumption in 72 h (n = 4 to 5 for each group), the ratio of NAD^+ to NADH (n = 4 for each group), and the levels of intracellular lactate (n = 4–5 for each group) in resting PMs.

Data information: Data are presented as mean ± s.e.m. (B and C). N represents biological replicates. P-values were determined by unpaired t-test. *P < 0.05; **P < 0.01; ***P < 0.001; n.s., not significant.
Source data are available online for this figure.

We proceeded to investigate whether targeting the lactate-ROS axis could serve as a potential therapeutic strategy to reverse the hyperinflammation observed in *Spns2*$^{-/-}$ sepsis models during the early stages of sepsis. Here, we established *Spns2*$^{-/-}$ sepsis models induced by intraperitoneal injection of heat-killed *E. coli*, which resulted in severe hyperinflammation (Fig EV1A and B), and administered oxamate and mitoquinone. Additionally, we used S1P to suppress the activity of the lactate-ROS axis from upstream. Remarkably, these treatments effectively alleviated hyperinflammation in *Spns2*$^{-/-}$ sepsis models, leading to the survival of all treated rats (Fig 7C). Overall, these findings provide *in vivo* evidence supporting our suggestion that the overactivity of the lactate-ROS axis is a vital mechanism driving hyperinflammation during the early stages of sepsis and underscore the importance of Spns2/S1P signaling in preventing uncontrolled inflammatory response by regulating the activity of the lactate-ROS axis.

Spns2/S1P signaling is necessary to sustain inflammation and to prevent innate immunosuppression

Despite the initial intense inflammation resulting from the lack of Spns2, immunosuppression rapidly occurred in PMs. This

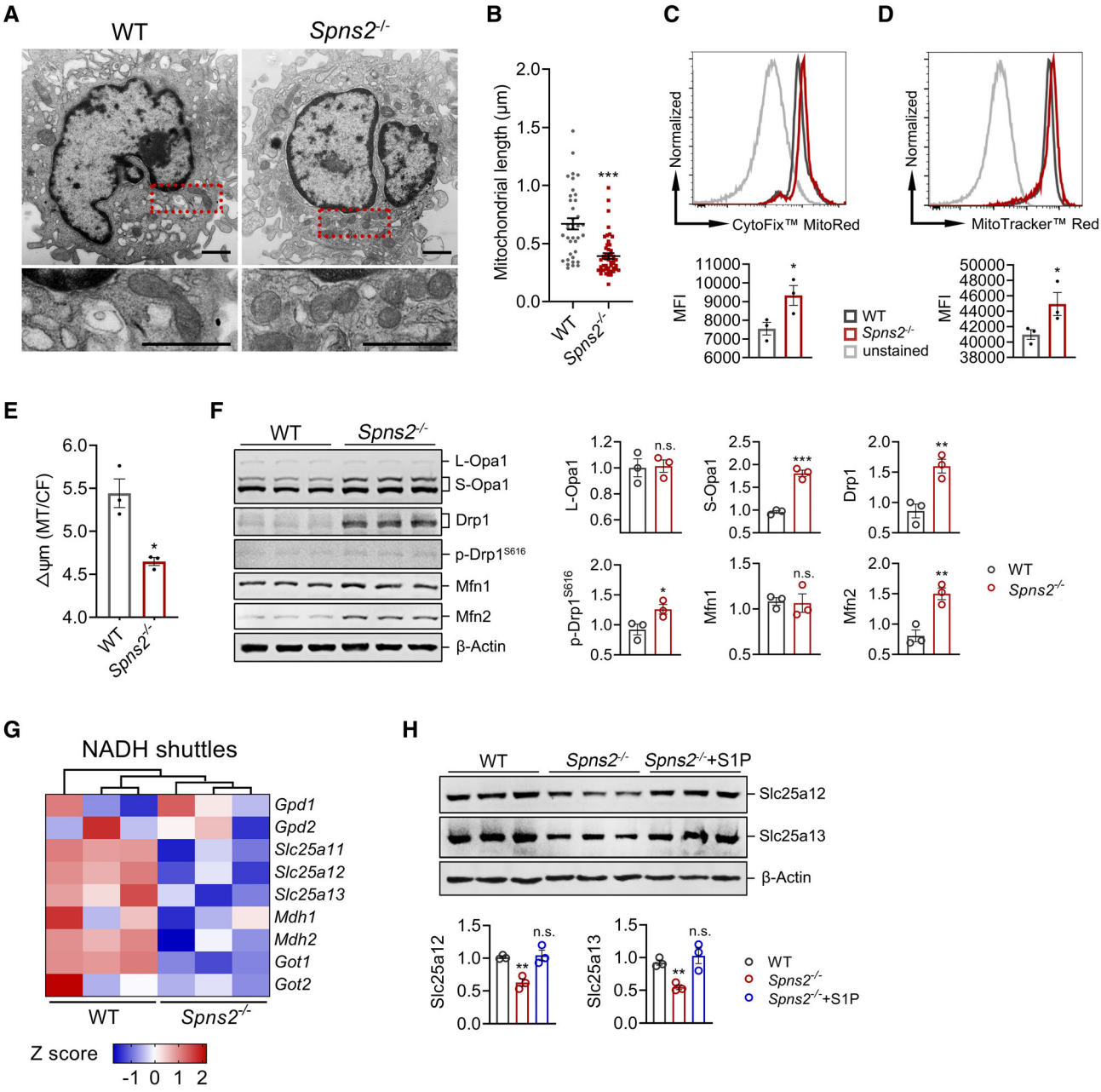

Figure 4. Spns2/S1P signaling regulates mitochondrial remodeling via the malate–aspartate shuttle.

A Fragmented mitochondrial morphology in *Spns2*$^{-/-}$ PMs revealed by transmission electron microscopy. Zoom-in view of the area in the red frame is shown below. Scale bars: 1 μm.

B The lengths of 38 and 47 mitochondria from WT and *Spns2*$^{-/-}$ PMs, respectively (n = 1 for each group).

C, D Flow cytometry analysis of mitochondrial mass probed by CytoFix™ MitoRed (CF, C) and mitochondrial membrane potential (Δψm) probed by MitoTracker™ Red (MT, D) in resting PMs (n = 3 for each group). MFI, mean fluorescent intensity.

E Average Δψm determined by the ratio of MFI_{MT} to MFI_{CF} (n = 3 for each group).

F The expression of proteins involved in mitochondrial dynamics (n = 3 for each group).

G Heat map displaying the gene expression of MAS and G3PS components (n = 3 for each group).

H Protein levels of Slc25a12 and Slc25a13 in WT, *Spns2*$^{-/-}$, and 1 μM S1P pretreated *Spns2*$^{-/-}$ PMs (n = 3 for each group).

Data information: Data are presented as mean ± s.e.m. (B–F and H). N represents biological replicates. P-values were determined by unpaired t-test. *P < 0.05; **P < 0.01; ***P < 0.001; n.s., not significant.
Source data are available online for this figure.

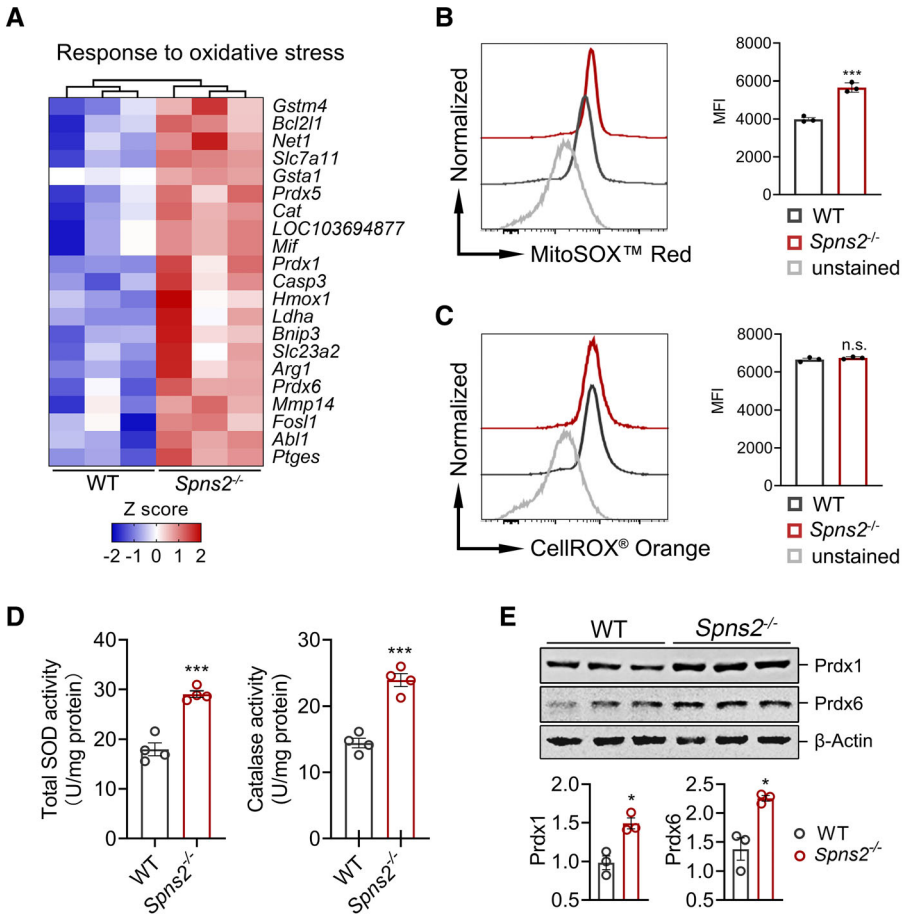

Figure 5. Spns2 deficiency leads to an altered redox state in resting peritoneal macrophages.

A Heat map showing the upregulated genes in *Spns2*$^{-/-}$ PMs associated with the response to oxidative stress (n = 3 for each group).

B, C Flow cytometry analysis of MitoSOX™ Red probed mitochondrial-derived ROS (mtROS) (B) and CellROX® Orange probed total intracellular ROS (C) in resting PMs (n = 3 for each group). MFI, mean fluorescent intensity.

D Activities of total superoxide dismutase (SOD) and catalase in resting PMs (n = 4 for each group).

E Protein levels of peroxiredoxin 1 (Prdx1) and Prdx6 in resting PMs (n = 3 per group).

Data information: Data are presented as mean ± s.e.m. (B–E). N represents biological replicates. P-values were determined by unpaired t-test. *P < 0.05; ***P < 0.001; n.s., not significant.
Source data are available online for this figure.

contributed to the high mortality observed in *Spns2*$^{-/-}$ CLP models without antibiotic therapy as well as the persistence of high levels of unresolved infection in *Spns2*$^{-/-}$ CLP models with antibiotic therapy. Given that intracellular lactate has been reported to promote macrophage homeostasis (Zhang *et al*, 2019), we investigated whether the brake on inflammation was related to metabolic changes. We observed a moderate increase in the level of intracellular lactate in *Spns2*$^{-/-}$ PMs compared with WT PMs at each time point after the LPS challenge (Fig EV5A). However, inhibiting the production of intracellular lactate in *Spns2*$^{-/-}$ PMs through oxamate only affected the intensity of initial inflammatory response and failed to restore the gene expression of pro-inflammatory cytokines after 3 h (Fig 7A). Furthermore, increasing the basal levels of intracellular lactate in WT PMs using rotenone intensified their immune response to LPS stimulation and failed to replicate the immunosuppression observed in *Spns2*$^{-/-}$ PMs during the later phase of infection, indicating the existence of a lactate-independent mechanism (Fig EV5B).

We hypothesized that the lack of Spns2 in macrophages led to unactivated S1PRs, resulting in a significant decrease in inflammation. The addition of S1P effectively restored the expression of *Il6* and *Il1β* in *Spns2*$^{-/-}$ PMs after 6-h postinfection (Fig 8A), indicating that Spns2 deficiency could potentially lead to immunosuppression in PMs. However, the expression of *Tnfα*, which exhibited a downward trend after 6 h, was not obviously affected by S1P supplementation in this model. Subsequently, we investigated whether improving S1P signaling activation would ameliorate immunosuppression and enhance the survival rate in septic rats. As the septic foci were primarily located in the peritoneal cavity for CLP models, *Spns2*$^{-/-}$ septic rats were treated with intraperitoneal injection of

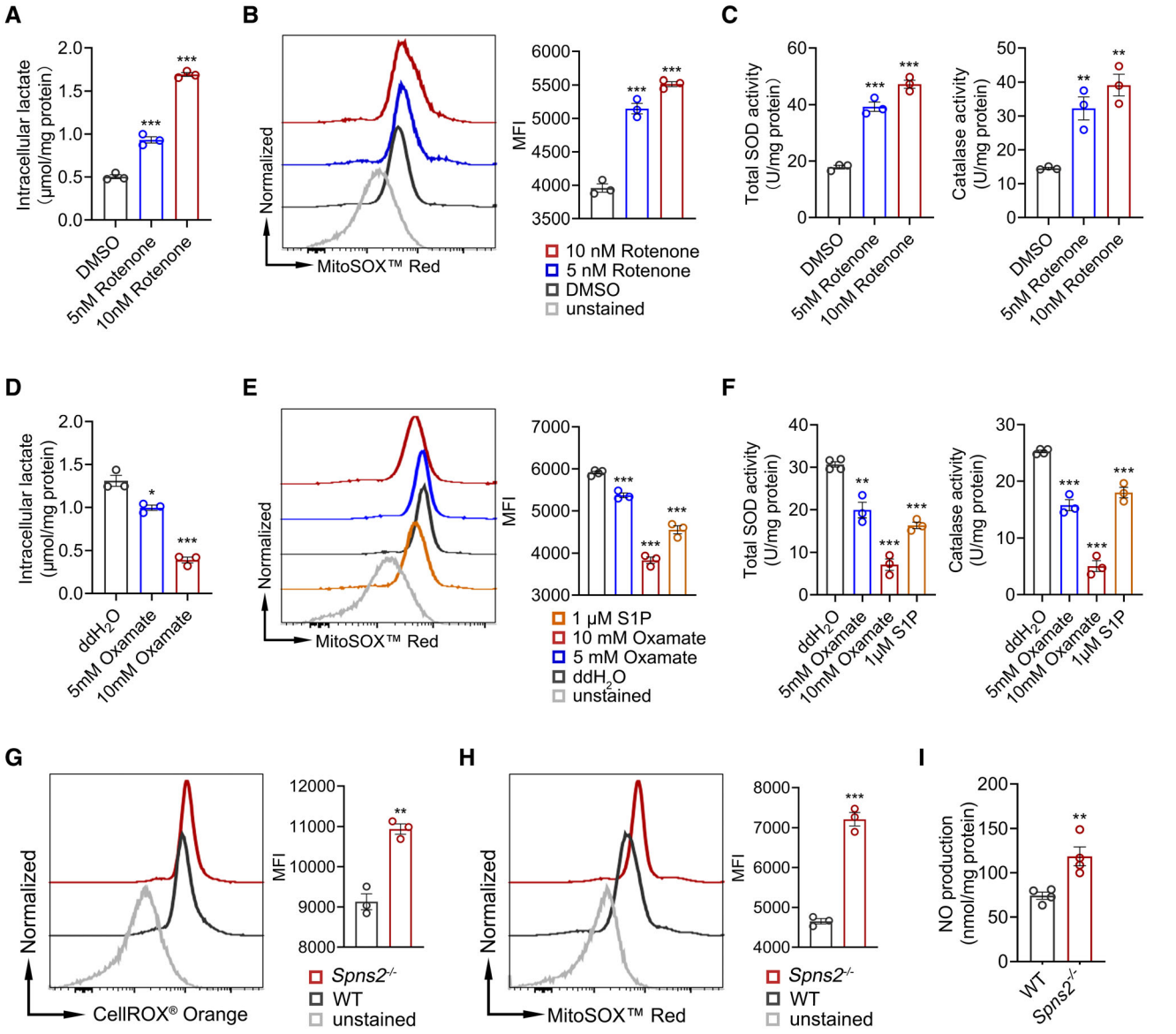

Figure 6. Intracellular lactate promotes mtROS generation in peritoneal macrophages.

A Elevated levels of intracellular lactate in resting WT PMs treated with 5 and 10 nM rotenone for 16 h (n = 3 for each group).

B Increased mtROS generation in rotenone-treated WT PMs probed by MitoSOX™ Red (n = 3 for each group).

C Enhanced activities of total superoxide dismutase (SOD) and catalase in rotenone-treated WT PMs (n = 3 for each group).

D Reduced levels of intracellular lactate in resting *Spns2*$^{-/-}$ PMs treated with 5 and 10 mM oxamate for 16 h (n = 3 for each group).

E Decreased mtROS generation in oxamate- and S1P-treated *Spns2*$^{-/-}$ PMs (n = 3–4 for each group).

F Attenuated activities of total SOD and catalase in oxamate- and S1P-treated *Spns2*$^{-/-}$ PMs (n = 3 to 4 for each group).

G, H Higher levels of both total cellular ROS (G, probed by CellROX® Orange) and mtROS (H, probed by MitoSOX™ Red) in *Spns2*$^{-/-}$ PMs challenged with 10 ng/ml LPS for 3 h (n = 3 for each group).

I Elevated production of nitric oxide (NO) by activated *Spns2*$^{-/-}$ PMs (n = 4 for each group).

Data information: Data are presented as mean ± s.e.m. N represents biological replicates. P-values were determined by unpaired t-test. *P < 0.05; **P < 0.01; ***P < 0.001.

Source data are available online for this figure.

S1P immediately after surgery, followed by twice-daily injections, to locally activate S1P signaling in PMs, while saline served as the control. Since the gene expression of *Spns2* in *Spns2*$^{+/-}$ PMs was approximately half that of WT PMs (Fig EV2D), we also tested whether partial recovery of Spns2 expression by using *Spns2*$^{+/-}$ rats could improve the survival in CLP models without antibiotic therapy. The results showed that S1P treatment and increased Spns2 expression significantly enhanced the survival rate and median

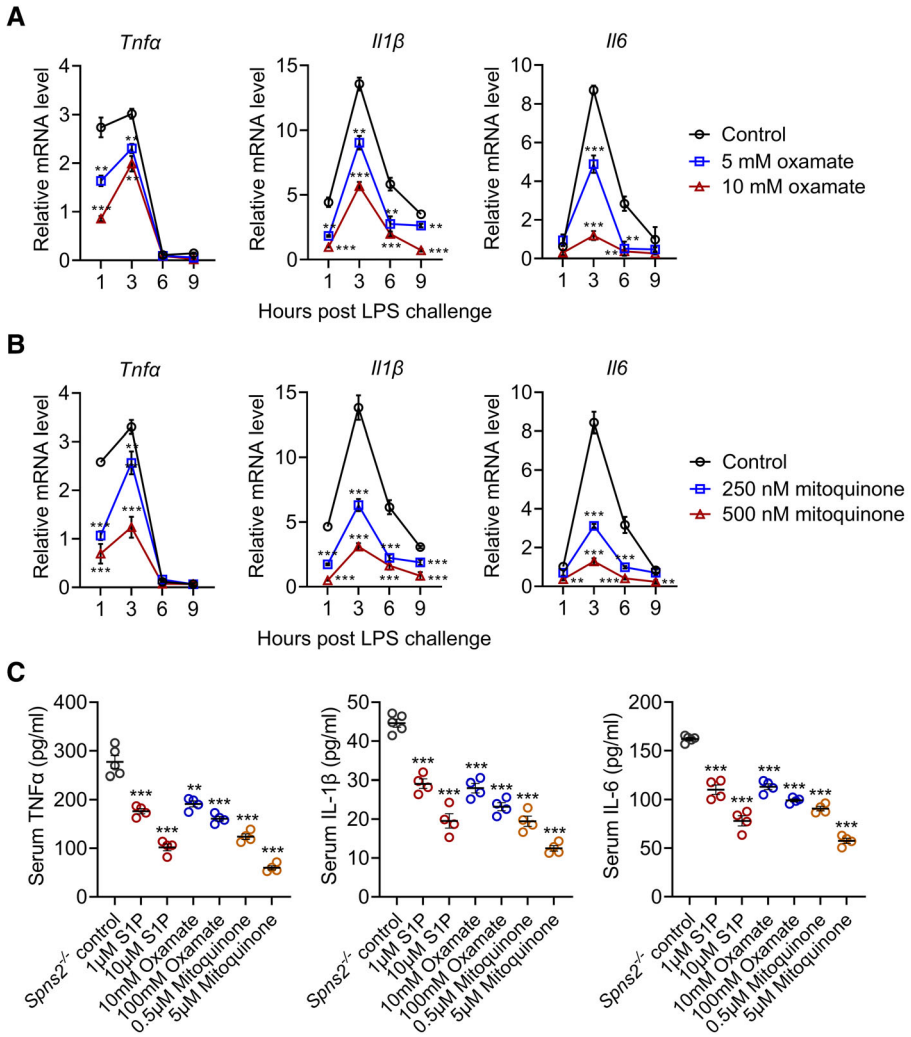

Figure 7. Spns2/S1P signaling alleviates hyperinflammation in sepsis through the lactate-ROS axis.

A, B Reduced gene expression of inflammatory cytokines in *Spns2*$^{-/-}$ PMs treated with either oxamate (A) or mitoquinone (B) (n = 3 per time point for each group).

C Activation of Spns2/S1P signaling and suppression of the lactate-ROS axis promoted the survival of *Spns2*$^{-/-}$ sepsis models induced by heat-killed *E. coli* through the alleviation of hyperinflammation (n = 5 for *Spns2*$^{-/-}$ control group; n = 4 for each treatment group).

Data information: Data are presented as mean ± s.e.m. N represents biological replicates. P-values were determined by unpaired t-test. $^{**}P < 0.01$; $^{***}P < 0.001$.
Source data are available online for this figure.

survival time of septic rats (Figs 8B and EV5C). These effects were closely related to the restoration of pro-inflammatory cytokine production measured at 12-h post-CLP (Fig 8C), highlighting the pivotal role of S1P signaling in sustaining inflammatory response and the potential therapeutic significance of S1P in septic patients experiencing immunosuppression.

In summary, our findings suggest that Spns2/S1P signaling plays an essential role in modulating the function of macrophages. First, in resting macrophages, Spns2/S1P signaling strengthens the function of MAS and promotes mitochondrial fusion to sustain the process of OXPHOS. Insufficient antivation of S1P signaling leads to enhanced glycolysis and accumulation of intracellular lactate, which primarily contributes to the intensity of the immune response to bacterial infection. Second, although Spns2/S1P signaling is not necessary for establishing an immune response, it sustains the capacity of macrophages to produce pro-inflammatory cytokines over a more extended period. Therefore, the deficiency of Spns2/S1P signaling could be a significant mechanism that potentially mediates sepsis-induced hyperinflammation and immunosuppression.

Discussion

Spns2 plays a key role in transporting S1P and is predominantly expressed in endothelial cells, which contributes to establish high circulating S1P concentrations ranging in the micromolar range (Obinata & Hla, 2019). The majority of blood-borne S1P is stably bound with chaperone proteins such as HDL and albumin, and S1P transfer from chaperones to S1PRs is essential for S1P signaling activation (O'Brien *et al*, 2009; Obinata & Hla, 2019). Thus, the high

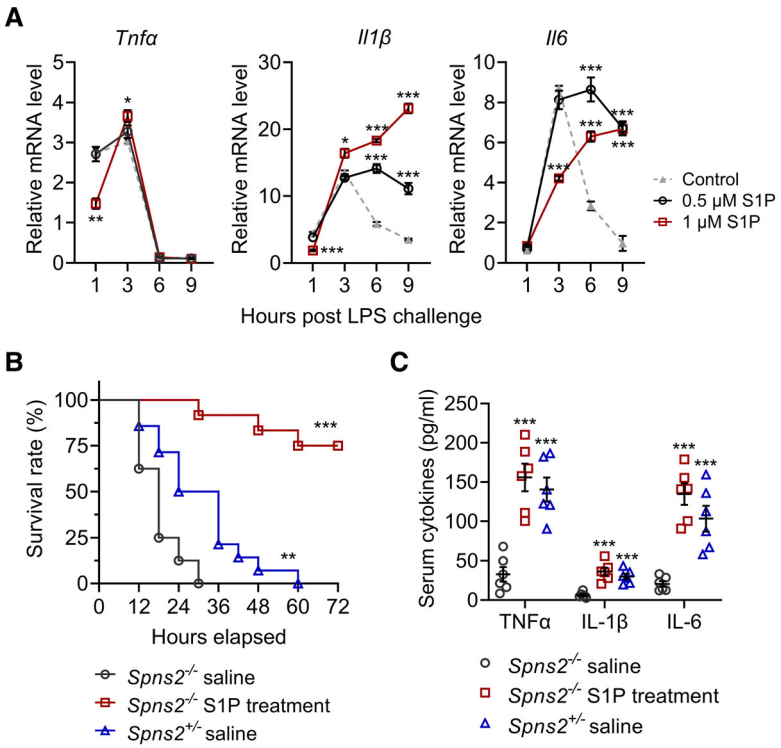

Figure 8. Spns2/S1P signaling prevents innate immunosuppression and improves outcomes in sepsis models.

A S1P treatment restored inflammatory response in *Spns2*$^{-/-}$ PMs after 6-h post-LPS challenge (n = 3 per time point for each group).

B Enhancement of Spns2/S1P signaling significantly improved the survival of CLP models without antibiotic therapy (n = 8 for *Spns2*$^{-/-}$ saline group; n = 14 for Spns2$^{+/-}$ group; n = 12 for *Spns2*$^{-/-}$ S1P treatment group).

C Enhancement of Spns2/S1P signaling restored inflammatory response in *Spns2*$^{-/-}$ CLP models at 12-h postinfection (n = 6 for each group).

Data information: Data are presented as mean ± s.e.m. (A and C) and percentage (B). *N* represents biological replicates. *P*-values were determined by unpaired *t*-test (A and C) and log-rank test (B). *$P < 0.05$; **$P < 0.01$; ***$P < 0.001$.
Source data are available online for this figure.

levels of blood-borne S1P are unable to cause broad activation of S1PRs, even though the K_d values for S1PR activation are ranging from only 8 to 50 nM. However, the mechanisms involved in the release of S1P from chaperones remain largely unknown, yet it is likely related to the hydrolysis of chaperones on the surface of recipient cells like endothelial cells (Tatematsu *et al*, 2013). During sepsis, the decrease in blood-borne S1P levels is primarily caused by the loss of HDL. This reduction may result in endothelial dysfunction and is inversely associated with disease severity and mortality (Winkler *et al*, 2015, 2017, 2019; Wu *et al*, 2019). However, little is known whether the changes in blood-borne S1P levels affected the innate immune response during sepsis. In this study, we propose that S1P secreted by macrophage-expressed Spns2, rather than circulating S1P bound with chaperone proteins, mainly contributed to the regulation of immune response during sepsis. Nevertheless, it remains uncertain whether changes in blood-borne S1P levels affect the innate immune response during sepsis. In this study, we propose that S1P secreted by macrophage-expressed Spns2 primarily contributes to regulating the immune response during sepsis, rather than circulating S1P bound with chaperone proteins.

We have identified Spns2 as an essential metabolic mediator in PMs that contributes to maintaining a proper balance in mitochondrial dynamics to produce sufficient ATP through OXPHOS. In the absence of Spns2, there is a significant impact on mitochondrial fusion, leading to enhanced aerobic glycolysis and increased levels of intracellular lactate (Mishra & Chan, 2016; Wai & Langer, 2016). Our research has shown that the absence of Spns2 results in increased levels of Drp1, p-Drp1^{S616}, and S-Opa1, which collectively contribute to morphological and functional changes in mitochondria of *Spns2*$^{-/-}$ PMs. Drp1 is a large GTPase that mediates the outer mitochondrial membrane (OMM) fission (Kraus *et al*, 2021). Recruited Drp1 and its adaptors (Fis1, MiD49, MiD50, and Mff) assemble mitochondrial divisome around OMM to mediate membrane constriction and scission in a GTP-dependent manner (Gandre-Babbe & van der Bliek, 2008; Otera *et al*, 2010; Palmer *et al*, 2011). In addition, phosphorylation of Drp1 at Ser616 can serve to increase the pro-fission activity of Drp1; thereby, the increased levels of both total Drp1 and p-Drp1^{S616} enhance mitochondrial fragmentation (Gandre-Babbe & van der Bliek, 2008; Guo *et al*, 2020; Kraus *et al*, 2021). Opa1 is initially expressed as L-Opa1 and can be cleaved by two peptidases (Oma1 and Yme1l) into S-Opa1, whose proteolytic regulation balances inner mitochondrial membrane (IMM) dynamics (Mishra & Chan, 2016). Blocking L-Opa1 processing to inhibit the production of S-Opa1 does not

enhance mitochondrial fusion, suggesting that the accumulation of L-Opa1 is dispensable for fusion (Anand *et al*, 2014). Instead, excess accumulation of S-Opa1 strongly accelerates mitochondrial fragmentation, indicating that S-Opa1 plays a critical role as a pro-fission mediator (Anand *et al*, 2014; Baker *et al*, 2014). We propose that the observed mitochondrial reorganization in *Spns2*$^{-/-}$ PMs may be attributed to compromised MAS function. Reports suggest that compromised MAS function leads to diminished mitochondrial $\Delta\psi m$ (Sanin *et al*, 2018), which is consistent with our observation. Notably, this decrease in mitochondrial $\Delta\psi m$ results in the activation of the potential-dependent protease Oma1, leading to the cleavage of L-Opa1 into S-Opa1 and ultimately contributing to mitochondrial fragmentation (Ehses *et al*, 2009; Head *et al*, 2009).

Studies have reported that mitochondrial reorganization in activated macrophages, including increased mass, fragmented morphology, and reduced $\Delta\psi$, is necessary for ROS generation and inflammatory cytokine production (Yu *et al*, 2020). However, the mechanisms by which the metabolic switch modulates the immune response require further elucidation. Additionally, the generation of ROS, which is essential for pathogen clearance, is considered to be closely related to the activation of Toll-like receptors (TLRs; West *et al*, 2011; Palikhe *et al*, 2019; Simpson *et al*, 2022). Nevertheless, we observed increased production of mtROS and antioxidative activity in resting *Spns2*$^{-/-}$ PMs, indicating a TLRs-independent mechanism that prompts oxidative stress. Our results suggest that intracellular lactate, which is a major product of glycolysis, promotes mtROS generation in both resting and activated macrophages, highlighting a positive role in the early stages of immune response. A recent study reports that lactate promotes a mild generation of ROS and triggers an antioxidative defense in neuroblastoma cells (Tauffenberger *et al*, 2019), which is similar to our finding that lactate is closely associated with the redox state in PMs. ROS target multiple essential pro-inflammatory pathways to stimulate cytokine production in activated macrophages (Canton *et al*, 2021). Notably, the excessive inflammation observed in the early phase of infection in *Spns2*$^{-/-}$ PMs was found to be linked with higher levels of ROS, while inhibition of lactate production resulted in the opposite effect. These findings suggest the critical pro-inflammatory role of intracellular lactate through the lactate-ROS axis.

Despite the excessive and lethal hyperinflammation observed during the early stages of sepsis in *Spns2*$^{-/-}$ rats, the subsequent immunosuppression is also an important finding that deserves attention. It has been reported that intracellular lactate can promote the expression of anti-inflammatory genes through a histone lactylation mechanism, leading to the suppression of the inflammatory response during the late phase of macrophage activation (Zhang *et al*, 2019). Our study suggests that Spns2 deficiency causes overactivity in the lactate-ROS axis, which results in hyperinflammatory response during the early stages of infection. Consequently, higher levels of intracellular lactate in *Spns2*$^{-/-}$ macrophages could potentially trigger severe immunosuppression. However, inhibiting the production of lactate did not reverse the occurrence of immunosuppression in *Spns2*$^{-/-}$ PMs. Notably, S1P treatment effectively restored the capacity of cytokine production in *Spns2*$^{-/-}$ PMs and significantly improved survival in *Spns2*$^{-/-}$ septic models. Hence, it is proposed that Spns2 deficiency is likely one of the major causes of innate immunosuppression in septic patients and could be a promising therapeutic target in sepsis.

Mfsd2b is another important S1P transported predominantly expressed in red blood cells (RBCs) and platelets. The absence of Mfsd2b in RBCs leads to a significant reduction in plasma S1P levels by approximately 50%. Additionally, Mfsd2b plays a critical role in RBC morphology, as knockout mice exhibited hemolysis associated with stomatocytes (Vu *et al*, 2017). In contrast, the lack of Mfsd2b in platelets does not cause decreased plasma S1P levels, but instead leads to platelet dysfunction due to the accumulation of S1P and other sphingomyelins (Chandrakanthan *et al*, 2021). This raises the question of whether Mfsd2b deficiency can affect immune response during sepsis. First, since Mfsd2b is not expressed in macrophages, it cannot mediate the activation of macrophage S1P signaling through S1P autocrine/paracrine, as Spns2 does. Second, Mfsd2b deficiency mainly causes a reduction in plasma S1P levels, which has limited impact on macrophage functions as demonstrated in this study. Third, since Mfsd2b in RBCs and platelets mediates the release of S1P, it is possible to affect monocytes/macrophages by S1P paracrine. However, our experiments have shown significant differences in immune response between WT and *Spns2*$^{-/-}$ sepsis models, despite Mfsd2b being unaffected. Therefore, it appears that the regulatory relationship between Mfsd2b-expressed cells and monocytes/macrophages does not play a major role in sepsis.

In summary, this study provides insight into the metabolic and immunomodulatory functions of Spns2/S1P signaling in macrophages and its fundamental impact on the immune response during sepsis. In the early stages of sepsis, Spns2/S1P signaling modulates the intensity of macrophage-mediated inflammation through the lactate-ROS axis. In the late stages, Spns2/S1P signaling is required to sustain the antibacterial response of macrophages, which is crucial for pathogen clearance. Notably, strengthening Spns2/S1P signaling contributes to balancing the immune response during sepsis, preventing both early hyperinflammation and later immunosuppression, making it a promising therapeutic target for sepsis. Further research is needed to understand the dynamic changes in the expression of Spns2 after infection, as well as the typical S1PRs that mediate both metabolic switch and immunomodulation, to fully comprehend the functions and therapeutic significance of Spns2/S1P signaling in sepsis.

Materials and Methods

Animal studies

Wild-type (WT) and *Spns2*$^{-/-}$ rats (Bian *et al*, 2018; Fang *et al*, 2018) were maintained in a specific-pathogen-free animal facility. All experimental procedures were performed under guidelines approved by the Animal Care and Use Committee of the Fourth Military Medical University.

Cecal ligation and puncture (CLP) models

Male rats aged 8–10 weeks weighing 200–220 g were used to generate CLP models following the previously reported protocol with modifications (Toscano *et al*, 2011). After anesthetizing, shaving, and disinfecting the abdomen, the cecum was exposed and tightly ligated with a 4–0 silk suture at a distance of 1.5 cm. The ligated cecum was perforated twice with an 18-gauge needle and gently

squeezed to extrude feces from the perforation sites. Buprenorphine (0.03 mg/kg) was subcutaneously injected for analgesia. Rats were monitored for survival every 6 h and euthanized at indicated endpoints.

To administer antibiotic therapy, CLP models were given 5 mg/ml meropenem in saline at a dose of 25 mg/kg through intraperitoneal injection immediately postsurgery, followed by twice-daily injections.

To administer S1P treatment, *Spns2*$^{-/-}$ rats were intraperitoneally injected with 2 ml of 10 μM S1P (Cayman Chemical, 62570) in sterile saline immediately after CLP, and 1 ml of 10 μM S1P in sterile saline every 12 h for maintenance. An equal amount of sterile saline was injected for the control group.

For colony-forming units (CFUs) counting, rats were euthanized at indicated time points after CLP, and the livers and spleens were harvested aseptically. The organs were weighed, homogenized in sterile saline solution, and plated on agar plates at appropriate dilutions. CFUs were counted after incubating for 18 h at 37°C and expressed as CFU/g.

Monomicrobial infection models

To conduct live *E. coli*-induced sepsis experiments, a bacterial suspension was prepared at a concentration of 2×10^9 CFU/ml and injected intraperitoneally into rats at a dose of 0.3 ml/100 g. To establish heat-killed *E.coli*-induced sepsis models, the bacterial suspension was heated at 68°C for 30 min prior to injection. In order to alleviate hyperinflammation observed during sepsis, heat-killed *E.coli*-induced *Spns2*$^{-/-}$ sepsis models were administered 1 ml of S1P at concentrations of 1 and 10 μM, oxamate (TargetMOI, T19831) at concentrations of 10 and 100 mM, or mitoquinone (MedChemExpress, HY-100116A) at concentrations of 0.5 and 5 μM via intraperitoneal injection immediately after infection. To simulate slow and continuous release of bacteria in CLP models, rats were given an intraperitoneal injection of a bacterial suspension containing 10^8 CFU/ml at a dose of 0.3 ml/100 g, followed by 0.05 ml/100 g of the suspension per hour for the next 11 h.

In *S. typhimurium* infection models, rats weighing between 200 and 220 g were intraperitoneally injected with 1,000 *S. typhimurium* in 500 μl saline. Rats were euthanized 1-, 3-, and 5-day postinfection, and their livers and spleens were harvested aseptically for CFU counting, as described above.

Bone marrow transplantation

Female rats weighing between 200 and 250 g were used as recipients. One week prior to irradiation, the recipients received acidic water (pH = 3) containing 32 mg/L gentamycin. The recipients were then irradiated with 8.5 Gy X-ray at a rate of 0.8 Gy/min in one dose. After 24 h, the recipients were given 2×10^7 mononuclear marrow cells from male rats aged 6–8 weeks old with different genotypes via tail vein injection. Transplantations were repeated three times with an interval of 24 h. The control animals were irradiated and left nontransplanted. The recipients were kept on acidic water containing 32 mg/l gentamycin and 500 mg/l ampicillin for 3 weeks after irradiation. Afterward, they were switched to acidic water without antibiotics for the rest of their lives. The recipients were kept for 6 weeks to allow complete immunological reconstitution. The chimerism rate was determined by the percentage of GFP$^+$ population in peritoneal cells and mononuclear marrow cells using flow cytometry.

Enzyme-linked immunosorbent assay (ELISA)

CLP rats were anesthetized, and blood was collected from the orbital sinus or tail vein at indicated time points. The serum was separated and used for the measurements of TNFα, IL-1β, IL-6 (ZCiBiO, ZC-37624, ZC-36391, and ZC-36404), and S1P (Echelon Biosciences, K-1900) by ELISA as per the manufacturer's instructions.

Peritoneal macrophages (PMs) isolation and stimulation

The isolation of PMs was performed as per the previously reported protocol with modification (Rios *et al*, 2017). Male rats aged 8–10 weeks weighing between 200 and 220 g were used for peritoneal cell extraction. The suspension was adjusted to 5×10^6 cells per ml in DMEM containing L-glutamine (Gibco, 11965), 10% fetal bovine serum (Hyclone, SH30070.03), 100 U/ml penicillin, and 100 μg/ml streptomycin (Gibco, 10378016). Cells were incubated at 37°C with 5% CO_2 for 1 h, and nonadherent cells were subsequently removed by gently washing with PBS. Purified PMs were incubated for another 2 h before proceeding to the next steps.

For the LPS (Ultrapure LPS, *E. coli* 0111:B4, InvivoGen) challenge, PMs were stimulated with either 1 or 10 ng/ml concentrations for the indicated duration and collected for further analysis. In some experiments, PMs were pretreated with 5 and 10 nM rotenone (TargetMOI, T2970), 5 and 10 mM oxamate, 0.5 and 1 μM S1P, or 250 and 500 nM mitoquinone for 16 h before proceeding to the next steps.

For the *in vitro S. typhimurium* infection, overnight bacterial cultures were washed with PBS and resuspended in the macrophage culture medium without antibiotics. PMs were washed with PBS and challenged by *S. typhimurium* at a multiplicity of infection of 50. Infected PMs were then washed with PBS after 30 min and incubated in the medium with 200 μg/ml gentamicin. At 2-h postinfection, PMs were washed with PBS and either incubated in medium with 20 μg/ml gentamicin for an additional 4 h or lysed with 1% Triton X-100 in PBS for CFUs counting. Intracellular *S. typhimurium* at 6-h postinfection was obtained in the same way, and the replication rate was calculated by the ratio of CFUs at 6 to 2 h.

Co-cultures of peritoneal macrophages and endothelial cells

Human umbilical vein endothelial cells (HUVECs) were cultured in the chambers of 0.4 μm pore transwell inserts (Corning, CLS3396) using endothelial cell medium (ScienCell, 1001). *Spns2*$^{-/-}$ PMs were isolated and cultured in macrophage culture medium as mentioned above in a 24-well plate. Once the HUVECs reached 90% confluency, the transwell inserts were transferred to the wells containing *Spns2*$^{-/-}$ PMs for a 12-h co-culture period. Subsequently, 10 ng/ml LPS was added to both chambers and PMs were harvested at indicated time points for further analysis.

RNA sequencing

Total RNA was extracted from PMs using TRIzol™ Reagent (Invitrogen) as per the manufacturer's instructions, and Illumina

Truseq™ RNA sample prep Kit was used to prepare libraries with an average size of 300 bp. The libraries were sequenced with an Illumina NovaSeq 6000 sequencer (2 × 150 bp read length). Fastp v.0.19.5 was used to trim and quality control the raw paired-end reads, and HISAT2 v.2.1.0 was used in orientation mode to map the clean reads to the reference genome. The mapped reads were assembled by StringTie v.2.1.2, and the expression level of each gene was calculated using the transcripts per million reads (TPM) method. Differential expression analysis was performed using DESeq2 v.1.24.0, and genes with fold-change ≥ 1.5 and *P*-adjust ≤ 0.05 were considered significant. Hierarchical clustering was carried out using Fastcluster v.1.2.6. Heat maps were generated using GraphPad Prism v.8.4.3. Gene Ontology (GO) enrichment analysis was performed by Goatools v.0.6.5.

Oxygen consumption rate (OCR)

To measure extracellular oxygen consumption, a Mitochondrial Stress Test Complete Assay Kit (Abcam, ab232857) was used as per the manufacturer's instructions with some modifications. First, PMs were plated in a 96-well flat clear bottom black microplate (Corning) following the procedure described above. The next day, the supernatant was replaced with 100 μl fresh culture medium containing the reconstituted extracellular O_2 probe. A final concentration of 1.5 μM oligomycin, 2.5 μM carbonyl cyanide-4-(trifluoromethoxy) phenylhydrazone (FCCP), or a combination of 1 μM antimycin A and 1 μM rotenone was added, respectively. Each well was then sealed with 100 μl prewarmed mineral oil, and the fluorescent intensity was immediately detected every 2 min for 30 min. The slopes (m) derived from the curves of signal profiles were indicative of OCR. Basal respiration rate was calculated as $m_{\text{untreated}} - m_{\text{antimycin A}}$. Maximal respiration rate was calculated as $m_{\text{FCCP}} - m_{\text{antimycin A}}$. ATP-coupled oxygen consumption was calculated as $m_{\text{untreated}} - m_{\text{oligomycin}}$. Non-ATP-coupled oxygen consumption (proton leak) was calculated as $m_{\text{oligomycin}} - m_{\text{antimycin A}}$. OCR data were normalized by protein quantification using Enhanced BCA Protein Assay Kit (Beyotime, P0010) as per the manufacturer's instructions.

Metabolite measurements

Intracellular lactate levels and the ratio of nicotinamide adenine dinucleotide (NAD^+) to the reduced form NADH were determined from the cell lysate by Lactate Colorimetric Assay Kit (Nanjing Jiancheng Bioengineering Institute, A019-2-1) and NAD^+/NADH Assay Kit with WST-8 (Beyotime, S0175) according to the manufacturer's instructions, respectively. Glucose levels and the production of nitric oxide (NO) in the culture medium were detected by Glucose Assay Kit with O-toluidine (Beyotime, S0201) and Griess Reagent kit (Beyotime, S0021) as per the manufacturer's instructions, respectively. Results for intracellular lactate, glucose consumption in 72 h, and NO production were normalized by protein quantification as described above.

Reactive oxygen species (ROS) measurements

To measure the levels of total cellular ROS and mitochondrial-derived ROS (mtROS), CellROX® Orange Reagent (Invitrogen, C10443) and MitoSOX™ Red (Invitrogen, M36008) fluorescent probes were used, respectively. PMs were stained with 5 μM of the respective fluorescent probes added to the culture medium and incubated at 37°C for 30 min. Following staining, cells were washed with PBS and removed from the plates by pipetting with cold PBS containing 1 mM EDTA. Mean fluorescent intensity (MFI) was determined by flow cytometry and analyzed using FlowJo v.10.

Antioxidant activities measurements

The antioxidant activities were determined from the cell lysate using the Total Superoxide Dismutase Assay Kit with WST-8 (Beyotime, S0101) and Catalase Assay Kit (Beyotime, S0051), as per the manufacturer's instructions. Results were normalized by protein quantification as described above.

Transmission electron microscopy (TEM)

PMs were cultured overnight and harvested using cell scrapers. Cells were pelleted and prefixed with 3% glutaraldehyde and then postfixed with 1% osmium tetroxide. Samples were subsequently dehydrated, infiltrated, and embedded. Semithin sections were stained with methylene blue, while ultrathin sections were stained with uranyl acetate and lead citrate. Observations were made using JEM-1400-FLASH transmission electron microscope. Mitochondrial length was analyzed using ImageJ v.1.53k.

Mitochondrial mass and membrane potential (Δψm) measurements

CytoFix™ MitoRed (AAT Bioquest, 23200) is a dye that selectively stains mitochondria independent of Δψm gradient and can be used for mitochondrial mass measurements. PMs were incubated with 1:500 dilution of the stock solution as per the manufacturer's instructions for 30 min at 37°C. MitoTracker™ Red CMXRos (Invitrogen, M7512) specifically probes mitochondria in a Δψm-dependent manner. PMs were incubated with a final concentration of 250 nM fluorescent probe in the culture medium at 37°C for 30 min. Cells were washed and removed from plates as described above. The MFI was measured by flow cytometry. The average Δψm was calculated by the ratio of $MFI_{\text{MitoTracker™ Red}}$ to $MFI_{\text{CytoFix™ MitoRed}}$.

Western blot

Cells were lysed using RIPA Lysis Buffer (Sangon Biotech, C500005) containing protease and phosphatase inhibitor cocktails (Mei5bio, MF182-plus, MF183). Protein quantification was conducted as described above. Twenty microgram total protein was separated with 10 or 12.5% SDS–PAGE electrophoresis and blotted to PVDF membranes (Millipore, ISEQ00010). Following blocking in 5% skim milk or 5% bovine serum albumin (BSA) in Tris-buffered saline Tween (TBST) at room temperature, the PVDF membranes were incubated overnight at 4°C with primary antibodies. Anti-Prdx1 (A16412), anti-Prdx6 (A2031), anti-Drp1 (A16661), anti-β-Actin (AC026), anti-Opa1 (A9833), anti-Mfn1 (A9880), anti-Mfn2 (A19678), anti-Slc25a12 (A11688), and anti-Slc25a13 (A12557) were purchased from ABclonal Technology. Anti-p-$Drp1^{S616}$ (12749) was purchased from Signalway Antibody. After washing with TBST, the

membranes were incubated with HRP-conjugated secondary antibodies for 1 h at room temperature. The membranes were washed with TBST and visualized using an ECL substrate (AccuRef Scientific, AP0081). The images were analyzed using ImageJ v.1.53k.

Quantitative PCR

Total RNA was isolated using the RNA Easy Fast Tissue/Cell Kit (Tiangen, DP451) as per the manufacturer's instructions. Reverse transcription was conducted using Novoscript Plus All-in-one 1st Strand cDNA Synthesis SuperMix (Novoprotein, E047-01). Quantitative PCR was performed using SYBR Green qPCR Master Mix (Bimake, B21702). Gene expression levels were normalized to *Arbp*. The primer sequences used for amplifying the specific genes were as follows: *Tnfα*, 5′-TGGCGTGTTCATCCGTTCT and 5′-TCAGCGTCT CGTGTGTTTCT; *Il-1β*, 5′-GGGATGATGACGACCTGCTA and 5′-CACTTGTTGGCTTATGTTCTGT; *Il-6*, 5′-CCCACCAGGAACGAAAGT CAA and 5′-CATCAGTCCCAAGAAGGCAAC; *Spns2*, 5′-GGCTCCGA GACATGAAGG and 5′-AGGCAGATGAAGATGGCAGAT; *Arbp*, 5′-TA GAGGGTGTCCGCAATGTG and 5′- CAGTGGGAAGGTGTAGTCA GTC.

Statistics

The results were presented as means ± s.e.m. Statistical differences were determined using GraphPad Prism v.8.4.3. Unpaired *t*-tests or log-rank tests were used for statistical evaluations. *P*-values less than 0.05 were considered statistically significant.

Data availability

The raw RNA-seq data have been deposited in the Sequence Read Archive (SRA) database with the accession PRJNA904828 (https://www.ncbi.nlm.nih.gov/sra/PRJNA904828).

Expanded View for this article is available online.

Acknowledgements
This work was supported by grants from the National Natural Science Foundation of China (Nos. 81903671 and 81673477).

Author contributions
Chao Fang: Conceptualization; resources; data curation; formal analysis; funding acquisition; validation; investigation; methodology; writing – original draft; project administration. **Pan Ren:** Data curation; formal analysis; validation; investigation; visualization. **Ganlan Bian:** Data curation; validation; investigation; visualization. **Jian Wang:** Conceptualization; resources; writing – review and editing. **Jiaxin Bai:** Validation; investigation. **Jiaxing Huang:** Validation; investigation. **Yixiao Ding:** Validation; investigation. **Xueyong Li:** Conceptualization; resources; supervision; methodology; project administration. **Mingkai Li:** Resources; supervision; project administration. **Zheng Hou:** Conceptualization; resources; data curation; supervision; funding acquisition; methodology; project administration; writing – review and editing.

Disclosure and competing interests statement
The authors declare that they have no conflict of interest.

References

Anand R, Wai T, Baker MJ, Kladt N, Schauss AC, Rugarli E, Langer T (2014) The i-AAA protease YME1L and OMA1 cleave OPA1 to balance mitochondrial fusion and fission. *J Cell Biol* 204: 919 – 929

Bailey JD, Diotallevi M, Nicol T, McNeill E, Shaw A, Chuaiphichai S, Hale A, Starr A, Nandi M, Stylianou E *et al* (2019) Nitric oxide modulates metabolic remodeling in inflammatory macrophages through TCA cycle regulation and Itaconate accumulation. *Cell Rep* 28: 218 – 230

Baker MJ, Lampe PA, Stojanovski D, Korwitz A, Anand R, Tatsuta T, Langer T (2014) Stress-induced OMA1 activation and autocatalytic turnover regulate OPA1-dependent mitochondrial dynamics. *EMBO J* 33: 578 – 593

Bian G, Yu C, Liu L, Fang C, Chen K, Ren P, Zhang Q, Liu F, Zhang K, Xue Q *et al* (2018) Sphingosine 1-phosphate stimulates eyelid closure in the developing rat by stimulating EGFR signaling. *Sci Signal* 11: eaat1470

Canton M, Sanchez-Rodriguez R, Spera I, Venegas FC, Favia M, Viola A, Castegna A (2021) Reactive oxygen species in macrophages: sources and targets. *Front Immunol* 12: 734229

Cartier A, Hla T (2019) Sphingosine 1-phosphate: lipid signaling in pathology and therapy. *Science* 366: eaar5551

Caslin HL, Abebayehu D, Pinette JA, Ryan JJ (2021) Lactate is a metabolic mediator that shapes immune cell fate and function. *Front Physiol* 12: 688485

Chandrakanthan M, Nguyen TQ, Hasan Z, Muralidharan S, Vu TM, Li AWL, Le UTN, Thi Thuy Ha H, Baik SH, Tan SH *et al* (2021) Deletion of Mfsd2b impairs thrombotic functions of platelets. *Nat Commun* 12: 2286

Cheng SC, Quintin J, Cramer RA, Shepardson KM, Saeed S, Kumar V, Giamarellos-Bourboulis EJ, Martens JH, Rao NA, Aghajanirefah A *et al* (2014) mTOR- and HIF-1alpha-mediated aerobic glycolysis as metabolic basis for trained immunity. *Science* 345: 1250684

Cheng SC, Scicluna BP, Arts RJ, Gresnigt MS, Lachmandas E, Giamarellos-Bourboulis EJ, Kox M, Manjeri GR, Wagenaars JA, Cremer OL *et al* (2016) Broad defects in the energy metabolism of leukocytes underlie immunoparalysis in sepsis. *Nat Immunol* 17: 406 – 413

Dejager L, Pinheiro I, Dejonckheere E, Libert C (2011) Cecal ligation and puncture: the gold standard model for polymicrobial sepsis? *Trends Microbiol* 19: 198 – 208

Dietl K, Renner K, Dettmer K, Timischl B, Eberhart K, Dorn C, Hellerbrand C, Kastenberger M, Kunz-Schughart LA, Oefner PJ *et al* (2010) Lactic acid and acidification inhibit TNF secretion and glycolysis of human monocytes. *J Immunol* 184: 1200 – 1209

Ehses S, Raschke I, Mancuso G, Bernacchia A, Geimer S, Tondera D, Martinou JC, Westermann B, Rugarli EI, Langer T (2009) Regulation of OPA1 processing and mitochondrial fusion by m-AAA protease isoenzymes and OMA1. *J Cell Biol* 187: 1023 – 1036

Errea A, Cayet D, Marchetti P, Tang C, Kluza J, Offermanns S, Sirard JC, Rumbo M (2016) Lactate inhibits the pro-inflammatory response and metabolic reprogramming in murine macrophages in a GPR81-independent manner. *PLoS One* 11: e0163694

Espinosa-Diez C, Miguel V, Mennerich D, Kietzmann T, Sanchez-Perez P, Cadenas S, Lamas S (2015) Antioxidant responses and cellular adjustments to oxidative stress. *Redox Biol* 6: 183 – 197

Fang C, Bian G, Ren P, Xiang J, Song J, Yu C, Zhang Q, Liu L, Chen K, Liu F *et al* (2018) S1P transporter SPNS2 regulates proper postnatal retinal morphogenesis. *FASEB J* 32: 3597 – 3613

Fukuhara S, Simmons S, Kawamura S, Inoue A, Orba Y, Tokudome T, Sunden Y, Arai Y, Moriwaki K, Ishida J *et al* (2012) The sphingosine-1-phosphate

transporter Spns2 expressed on endothelial cells regulates lymphocyte trafficking in mice. *J Clin Invest* 122: 1416 – 1426

Gandre-Babbe S, van der Bliek AM (2008) The novel tail-anchored membrane protein Mff controls mitochondrial and peroxisomal fission in mammalian cells. *Mol Biol Cell* 19: 2402 – 2412

Guo L, Cui C, Wang J, Yuan J, Yang Q, Zhang P, Su W, Bao R, Ran J, Wu C (2020) PINCH-1 regulates mitochondrial dynamics to promote proline synthesis and tumor growth. *Nat Commun* 11: 4913

Head B, Griparic L, Amiri M, Gandre-Babbe S, van der Bliek AM (2009) Inducible proteolytic inactivation of OPA1 mediated by the OMA1 protease in mammalian cells. *J Cell Biol* 187: 959 – 966

Hoque R, Farooq A, Ghani A, Gorelick F, Mehal WZ (2014) Lactate reduces liver and pancreatic injury in toll-like receptor- and inflammasome-mediated inflammation via GPR81-mediated suppression of innate immunity. *Gastroenterology* 146: 1763 – 1774

Hotchkiss RS, Monneret G, Payen D (2013) Immunosuppression in sepsis: a novel understanding of the disorder and a new therapeutic approach. *Lancet Infect Dis* 13: 260 – 268

Hotchkiss RS, Moldawer LL, Opal SM, Reinhart K, Turnbull IR, Vincent JL (2016) Sepsis and septic shock. *Nat Rev Dis Primers* 2: 16045

Hou J, Chen Q, Zhang K, Cheng B, Xie G, Wu X, Luo C, Chen L, Liu H, Zhao B *et al* (2015) Sphingosine 1-phosphate receptor 2 signaling suppresses macrophage phagocytosis and impairs host defense against sepsis. *Anesthesiology* 123: 409 – 422

Hou J, Chen Q, Wu X, Zhao D, Reuveni H, Licht T, Xu M, Hu H, Hoeft A, Ben-Sasson SA *et al* (2017) S1PR3 signaling drives bacterial killing and is required for survival in bacterial sepsis. *Am J Respir Crit Care Med* 196: 1559 – 1570

Ishii T (2015) Close teamwork between Nrf2 and peroxiredoxins 1 and 6 for the regulation of prostaglandin D2 and E2 production in macrophages in acute inflammation. *Free Radic Biol Med* 88: 189 – 198

Kampjut D, Sazanov LA (2020) The coupling mechanism of mammalian respiratory complex I. *Science* 370: eabc4209

Kraus F, Roy K, Pucadyil TJ, Ryan MT (2021) Function and regulation of the divisome for mitochondrial fission. *Nature* 590: 57 – 66

Langston PK, Nambu A, Jung J, Shibata M, Aksoylar HI, Lei J, Xu P, Doan MT, Jiang H, MacArthur MR *et al* (2019) Glycerol phosphate shuttle enzyme GPD2 regulates macrophage inflammatory responses. *Nat Immunol* 20: 1186 – 1195

Lin HC, Chen YJ, Wei YH, Lin HA, Chen CC, Liu TF, Hsieh YL, Huang KY, Lin KH, Wang HH *et al* (2021) Lactic acid fermentation is required for NLRP3 Inflammasome activation. *Front Immunol* 12: 630380

Mendoza A, Breart B, Ramos-Perez WD, Pitt LA, Gobert M, Sunkara M, Lafaille JJ, Morris AJ, Schwab SR (2012) The transporter Spns2 is required for secretion of lymph but not plasma sphingosine-1-phosphate. *Cell Rep* 2: 1104 – 1110

Mishra P, Chan DC (2016) Metabolic regulation of mitochondrial dynamics. *J Cell Biol* 212: 379 – 387

Murray PJ (2020) On macrophage diversity and inflammatory metabolic timers. *Nat Rev Immunol* 20: 89 – 90

Nijnik A, Clare S, Hale C, Chen J, Raisen C, Mottram L, Lucas M, Estabel J, Ryder E, Adissu H *et al* (2012) The role of sphingosine-1-phosphate transporter Spns2 in immune system function. *J Immunol* 189: 102 – 111

Nolt B, Tu F, Wang X, Ha T, Winter R, Williams DL, Li C (2018) Lactate and immunosuppression in sepsis. *Shock* 49: 120 – 125

Obinata H, Hla T (2019) Sphingosine 1-phosphate and inflammation. *Int Immunol* 31: 617 – 625

O'Brien N, Jones ST, Williams DG, Cunningham HB, Moreno K, Visentin B, Gentile A, Vekich J, Shestowsky W, Hiraiwa M *et al* (2009) Production and characterization of monoclonal anti-sphingosine-1-phosphate antibodies. *J Lipid Res* 50: 2245 – 2257

Otera H, Wang C, Cleland MM, Setoguchi K, Yokota S, Youle RJ, Mihara K (2010) Mff is an essential factor for mitochondrial recruitment of Drp1 during mitochondrial fission in mammalian cells. *J Cell Biol* 191: 1141 – 1158

Otto GP, Sossdorf M, Claus RA, Rodel J, Menge K, Reinhart K, Bauer M, Riedemann NC (2011) The late phase of sepsis is characterized by an increased microbiological burden and death rate. *Crit Care* 15: R183

Palikhe S, Ohashi W, Sakamoto T, Hattori K, Kawakami M, Andoh T, Yamazaki H, Hattori Y (2019) Regulatory role of GRK2 in the TLR signaling-mediated iNOS induction pathway in microglial cells. *Front Pharmacol* 10: 59

Palmer CS, Osellame LD, Laine D, Koutsopoulos OS, Frazier AE, Ryan MT (2011) MiD49 and MiD51, new components of the mitochondrial fission machinery. *EMBO Rep* 12: 565 – 573

Peter K, Rehli M, Singer K, Renner-Sattler K, Kreutz M (2015) Lactic acid delays the inflammatory response of human monocytes. *Biochem Biophys Res Commun* 457: 412 – 418

van der Poll T, van de Veerdonk FL, Scicluna BP, Netea MG (2017) The immunopathology of sepsis and potential therapeutic targets. *Nat Rev Immunol* 17: 407 – 420

Rios FJ, Touyz RM, Montezano AC (2017) Isolation and differentiation of murine macrophages. *Methods Mol Biol* 1527: 297 – 309

Romero CR, Herzig DS, Etogo A, Nunez J, Mahmoudizad R, Fang G, Murphey ED, Toliver-Kinsky T, Sherwood ER (2010) The role of interferon-gamma in the pathogenesis of acute intra-abdominal sepsis. *J Leukoc Biol* 88: 725 – 735

Rosenberg G, Riquelme S, Prince A, Avraham R (2022) Immunometabolic crosstalk during bacterial infection. *Nat Microbiol* 7: 497 – 507

Rudd KE, Johnson SC, Agesa KM, Shackelford KA, Tsoi D, Kievlan DR, Colombara DV, Ikuta KS, Kissoon N, Finfer S *et al* (2020) Global, regional, and national sepsis incidence and mortality, 1990–2017: analysis for the global burden of disease study. *Lancet* 395: 200 – 211

Sanin DE, Matsushita M, Klein Geltink RI, Grzes KM, van Teijlingen BN, Corrado M, Kabat AM, Buck MD, Qiu J, Lawless SJ *et al* (2018) Mitochondrial membrane potential regulates nuclear gene expression in macrophages exposed to prostaglandin E2. *Immunity* 49: 1021 – 1033

Schuster S, Ewald J, Kaleta C (2021) Modeling the energy metabolism in immune cells. *Curr Opin Biotechnol* 68: 282 – 291

Shalova IN, Lim JY, Chittezhath M, Zinkernagel AS, Beasley F, Hernandez-Jimenez E, Toledano V, Cubillos-Zapata C, Rapisarda A, Chen J *et al* (2015) Human monocytes undergo functional re-programming during sepsis mediated by hypoxia-inducible factor-1alpha. *Immunity* 42: 484 – 498

Simmons S, Ishii M (2014) Sphingosine-1-phosphate: a master regulator of lymphocyte egress and immunity. *Arch Immunol Ther Exp (Warsz)* 62: 103 – 115

Simpson DS, Pang J, Weir A, Kong IY, Fritsch M, Rashidi M, Cooney JP, Davidson KC, Speir M, Djajawi TM *et al* (2022) Interferon-gamma primes macrophages for pathogen ligand-induced killing via a caspase-8 and mitochondrial cell death pathway. *Immunity* 55: e429

Singer M, Deutschman CS, Seymour CW, Shankar-Hari M, Annane D, Bauer M, Bellomo R, Bernard GR, Chiche JD, Coopersmith CM *et al* (2016) The third international consensus definitions for sepsis and septic shock (Sepsis-3). *JAMA* 315: 801 – 810

Song F, Hou J, Chen Z, Cheng B, Lei R, Cui P, Sun Y, Wang H, Fang X (2018) Sphingosine-1-phosphate receptor 2 signaling promotes Caspase-11-dependent macrophage Pyroptosis and worsens *Escherichia coli* sepsis outcome. *Anesthesiology* 129: 311 – 320

Steinhagen F, Schmidt SV, Schewe JC, Peukert K, Klinman DM, Bode C (2020) Immunotherapy in sepsis – brake or accelerate? *Pharmacol Ther* 208: 107476

Tatematsu S, Francis SA, Natarajan P, Rader DJ, Saghatelian A, Brown JD, Michel T, Plutzky J (2013) Endothelial lipase is a critical determinant of high-density lipoprotein-stimulated sphingosine 1-phosphate-dependent signaling in vascular endothelium. *Arterioscler Thromb Vasc Biol* 33: 1788 – 1794

Tauffenberger A, Fiumelli H, Almustafa S, Magistretti PJ (2019) Lactate and pyruvate promote oxidative stress resistance through hormetic ROS signaling. *Cell Death Dis* 10: 653

Torgersen C, Moser P, Luckner G, Mayr V, Jochberger S, Hasibeder WR, Dunser MW (2009) Macroscopic postmortem findings in 235 surgical intensive care patients with sepsis. *Anesth Analg* 108: 1841 – 1847

Toscano MG, Ganea D, Gamero AM (2011) Cecal ligation puncture procedure. *J Vis Exp* 51: 2860

Tur J, Vico T, Lloberas J, Zorzano A, Celada A (2017) Macrophages and mitochondria: a critical interplay between metabolism, signaling, and the functional activity. *Adv Immunol* 133: 1 – 36

Tur J, Pereira-Lopes S, Vico T, Marin EA, Munoz JP, Hernandez-Alvarez M, Cardona PJ, Zorzano A, Lloberas J, Celada A (2020) Mitofusin 2 in macrophages links mitochondrial ROS production, cytokine release, phagocytosis, autophagy, and bactericidal activity. *Cell Rep* 32: 108079

Venet F, Monneret G (2018) Advances in the understanding and treatment of sepsis-induced immunosuppression. *Nat Rev Nephrol* 14: 121 – 137

Venet F, Demaret J, Gossez M, Monneret G (2021) Myeloid cells in sepsis-acquired immunodeficiency. *Ann N Y Acad Sci* 1499: 3 – 17

Vu TM, Ishizu AN, Foo JC, Toh XR, Zhang F, Whee DM, Torta F, Cazenave-Gassiot A, Matsumura T, Kim S *et al* (2017) Mfsd2b is essential for the sphingosine-1-phosphate export in erythrocytes and platelets. *Nature* 550: 524 – 528

Wai T, Langer T (2016) Mitochondrial dynamics and metabolic regulation. *Trends Endocrinol Metab* 27: 105 – 117

Wang Y, Stancliffe E, Fowle-Grider R, Wang R, Wang C, Schwaiger-Haber M, Shriver LP, Patti GJ (2022) Saturation of the mitochondrial NADH shuttles drives aerobic glycolysis in proliferating cells. *Mol Cell* 82: 3270 – 3283

Weinberg SE, Sena LA, Chandel NS (2015) Mitochondria in the regulation of innate and adaptive immunity. *Immunity* 42: 406 – 417

West AP, Brodsky IE, Rahner C, Woo DK, Erdjument-Bromage H, Tempst P, Walsh MC, Choi Y, Shadel GS, Ghosh S (2011) TLR signalling augments macrophage bactericidal activity through mitochondrial ROS. *Nature* 472: 476 – 480

Willems PH, Rossignol R, Dieteren CE, Murphy MP, Koopman WJ (2015) Redox homeostasis and mitochondrial dynamics. *Cell Metab* 22: 207 – 218

Winkler MS, Nierhaus A, Holzmann M, Mudersbach E, Bauer A, Robbe L, Zahrte C, Geffken M, Peine S, Schwedhelm E *et al* (2015) Decreased serum concentrations of sphingosine-1-phosphate in sepsis. *Crit Care* 19: 372

Winkler MS, Nierhaus A, Poppe A, Greiwe G, Graler MH, Daum G (2017) Sphingosine-1-phosphate: a potential biomarker and therapeutic target for endothelial dysfunction and sepsis? *Shock* 47: 666 – 672

Winkler MS, Martz KB, Nierhaus A, Daum G, Schwedhelm E, Kluge S, Graler MH (2019) Loss of sphingosine 1-phosphate (S1P) in septic shock is predominantly caused by decreased levels of high-density lipoproteins (HDL). *J Intensive Care* 7: 23

Wu X, Hou J, Li H, Xie G, Zhang X, Zheng J, Wang J, Gao F, Yao Y, Liu H *et al* (2019) Inverse correlation between plasma Sphingosine-1-phosphate and ceramide concentrations in septic patients and their utility in predicting mortality. *Shock* 51: 718 – 724

Wu R, Chen F, Wang N, Tang D, Kang R (2020) ACOD1 in immunometabolism and disease. *Cell Mol Immunol* 17: 822 – 833

Xie JH, Li YY, Jin J (2020) The essential functions of mitochondrial dynamics in immune cells. *Cell Mol Immunol* 17: 712 – 721

Xu J, Gao C, He Y, Fang X, Sun D, Peng Z, Xiao H, Sun M, Zhang P, Zhou T *et al* (2022) NLRC3 expression in macrophage impairs glycolysis and host immune defense by modulating the NF-kappaB-NFAT5 complex during septic immunosuppression. *Mol Ther* 31: 154 – 173

Yang K, Xu J, Fan M, Tu F, Wang X, Ha T, Williams DL, Li C (2020) Lactate suppresses macrophage pro-inflammatory response to LPS stimulation by inhibition of YAP and NF-kappaB activation via GPR81-mediated signaling. *Front Immunol* 11: 587913

Young A, Oldford C, Mailloux RJ (2020) Lactate dehydrogenase supports lactate oxidation in mitochondria isolated from different mouse tissues. *Redox Biol* 28: 101339

Yu W, Wang X, Zhao J, Liu R, Liu J, Wang Z, Peng J, Wu H, Zhang X, Long Z *et al* (2020) Stat2-Drp1 mediated mitochondrial mass increase is necessary for pro-inflammatory differentiation of macrophages. *Redox Biol* 37: 101761

Zhang D, Tang Z, Huang H, Zhou G, Cui C, Weng Y, Liu W, Kim S, Lee S, Perez-Neut M *et al* (2019) Metabolic regulation of gene expression by histone lactylation. *Nature* 574: 575 – 580